Supplementary Figure 1

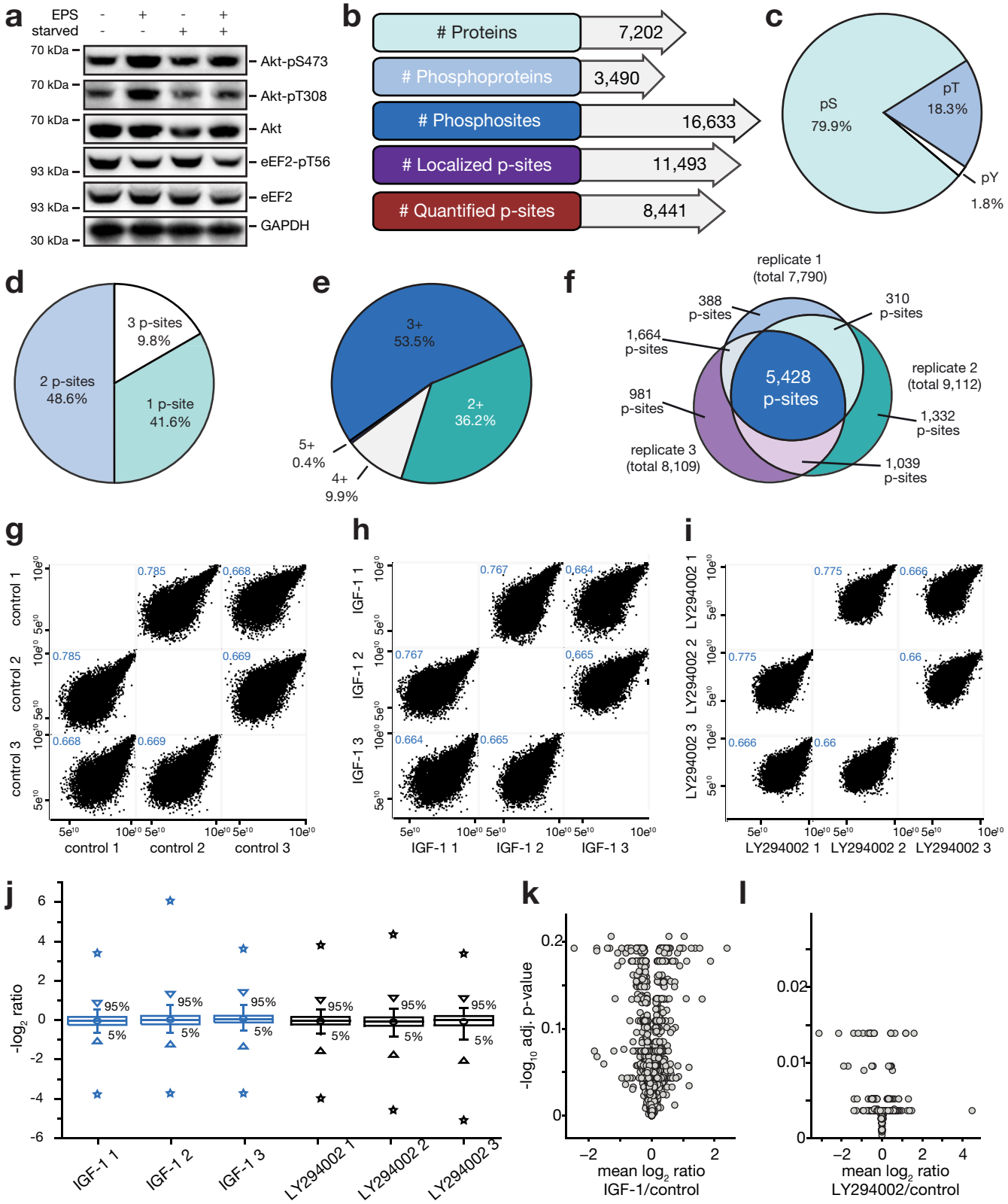

Supplementary Figure 1. Evaluation of quantitative phosphoproteome data from mouse skeletal myotubes follwoing treatment with IGF-1 or LY294002. **a.** C2 myotubes were starved over night and treated with EPS for 4 h. Lysates were subjected to SDS-PAGE and immunoblot analysis using total and phospho-specific antibodies. **b.** Overview of the number of identified proteins and phosphoproteins as well as the number of counted, localized (≥ 0.75) and quantified phospho-sites obtained by SILAC-MS and MaxQuant data analysis. **c.** Distribution of peptides identified to be phosphorylated at serine (pS) threonine (pT) or tyrosine (pY). **d.** Distribution of singly, doubly and triply phosphorylated peptides. **e.** Distribution of the charge state of phosphopeptides. **f.** Overlap of localized and quantified phosphosites between independent experiments. In sum, 8,441 phosphosites (73%) of all localized sites were quantified in two out of three replicates. **g-i.** Multi-scatter plots with Pearson correlation analysis between biological replicates for each condition (i.e. control, IGF-1 and LY294002 treatment). **j.** Box-plot analysis of log_2-transformed phosphopeptide ratios in replicates 1-3. Only a small fraction of all quantified phosphopeptides exhibits a log_2 ratio ≥ 0.584 or ≤ -0.584 (i.e. minimum fold-change of 1.5). **k and l.** Scatter plots of quantified proteins after 1 h treatment with IGF-1 (k) and LY294002 (l) in comparison to DMSO-treated control. No changes in the relative abundance of proteins were found (n=3 independent experiments; two-tailed moderated student's t-test).

Supplementary Figure 2

quantified

quantified and shown in Fig. 1b

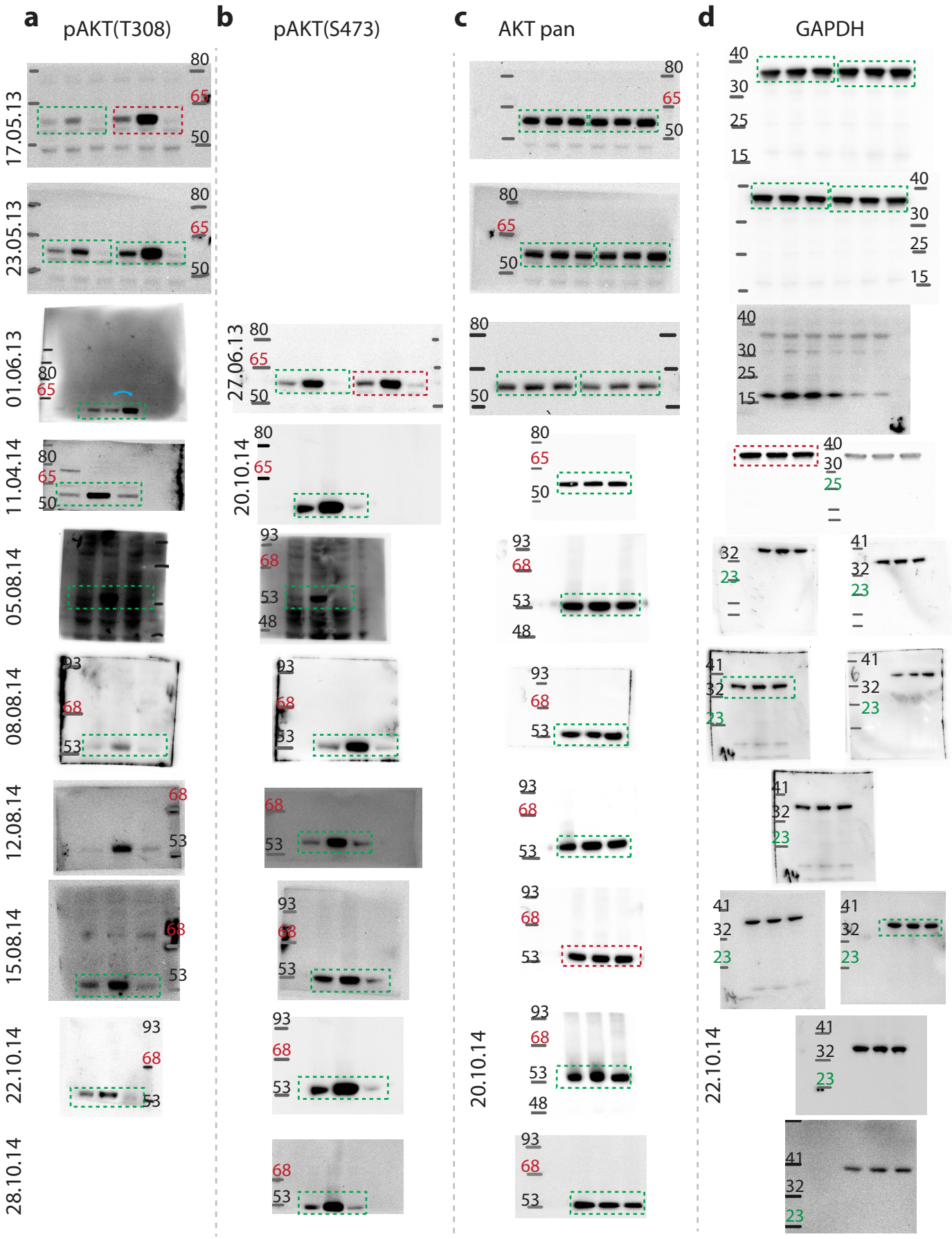

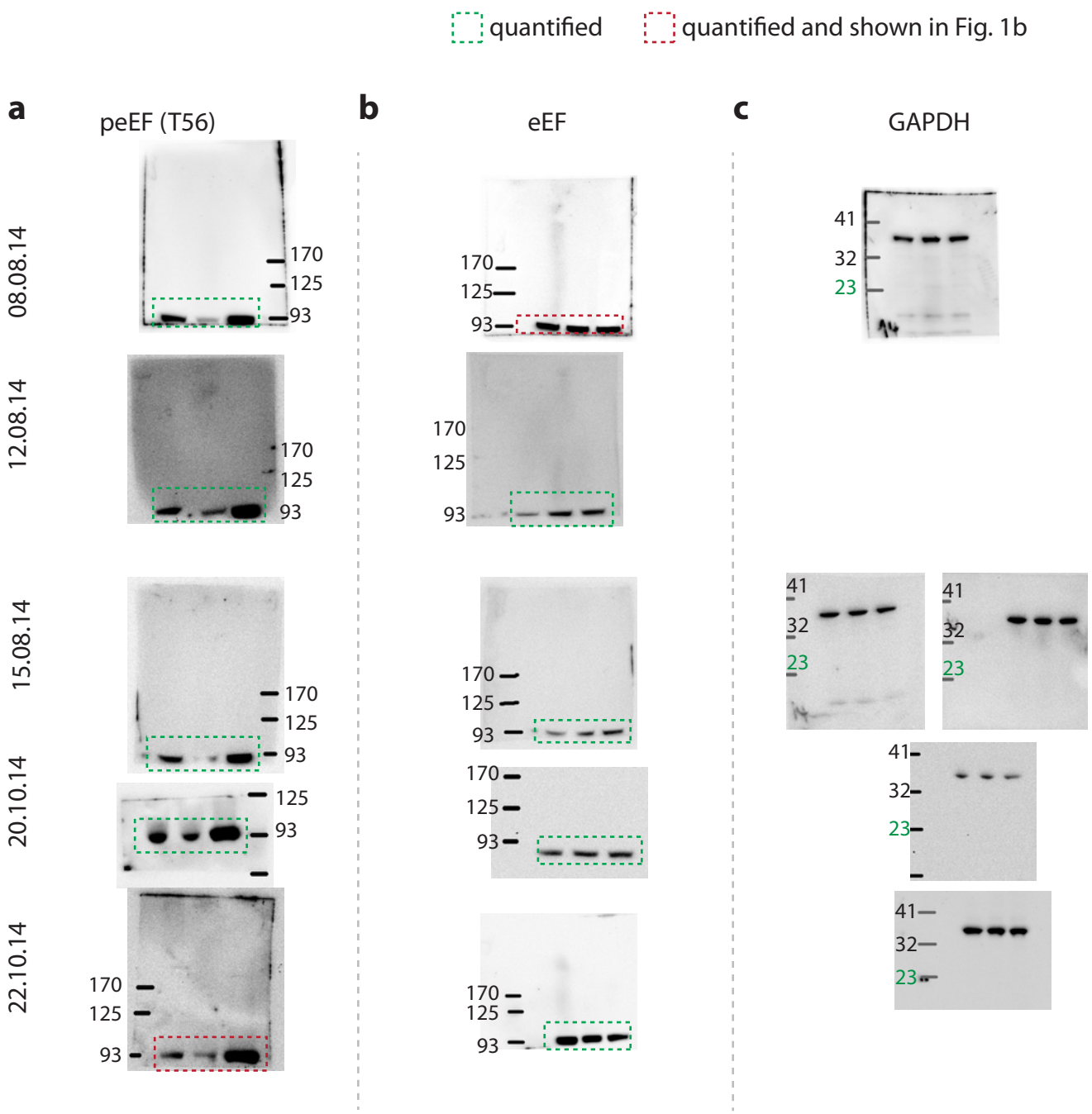
quantified
quantified and shown in Fig. 1b
a
peEF (T56)
b
eEF
c
GAPDH
08.08.14
12.08.14
15.08.14
20.10.14
22.10.14
170
125
93
41
32
23

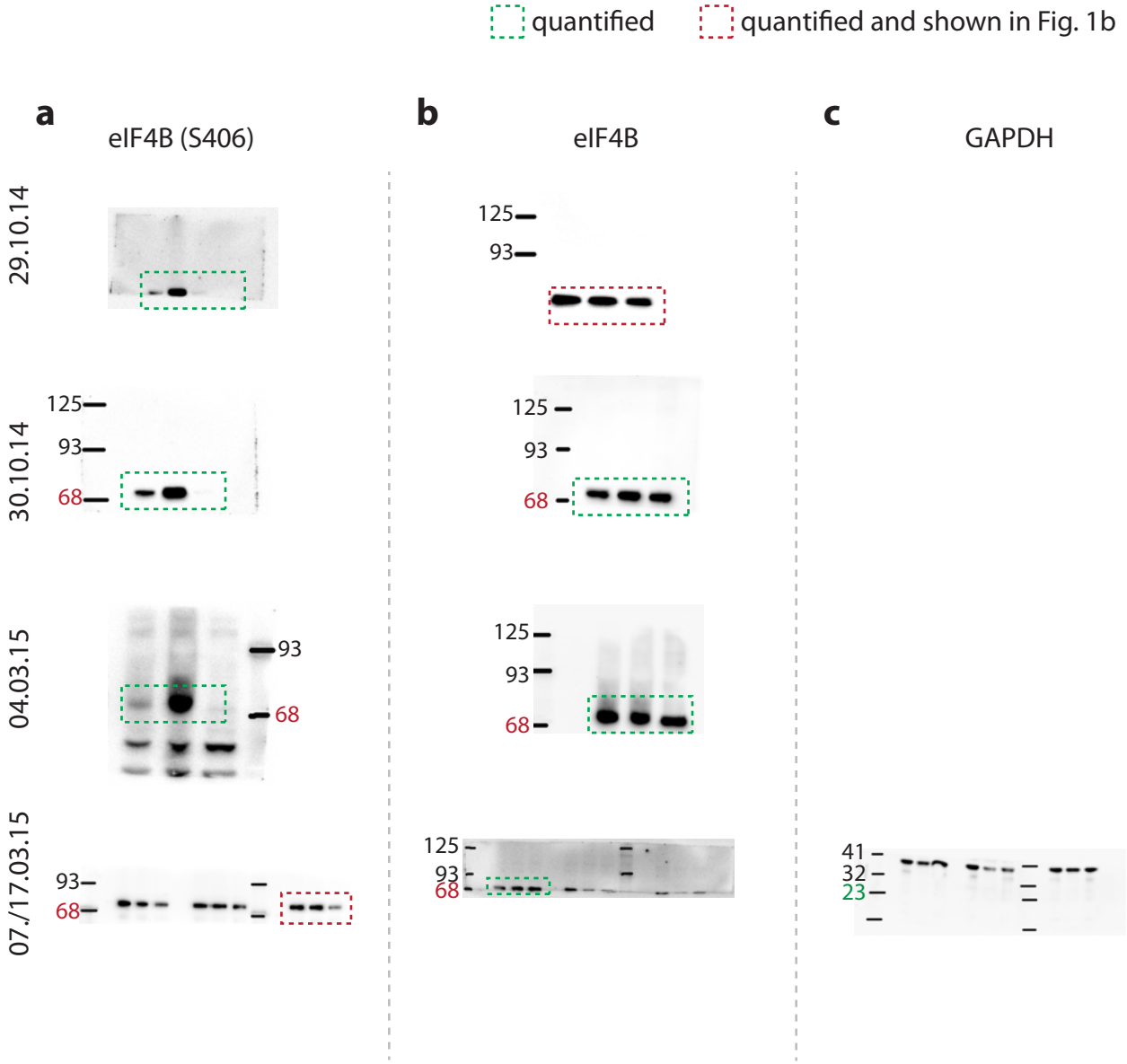
quantified
quantified and shown in Fig. 1b
a
eIF4B (S406)
b
eIF4B
c
GAPDH
29.10.14
30.10.14
04.03.15
07./17.03.15
125
93
68
41
32
23

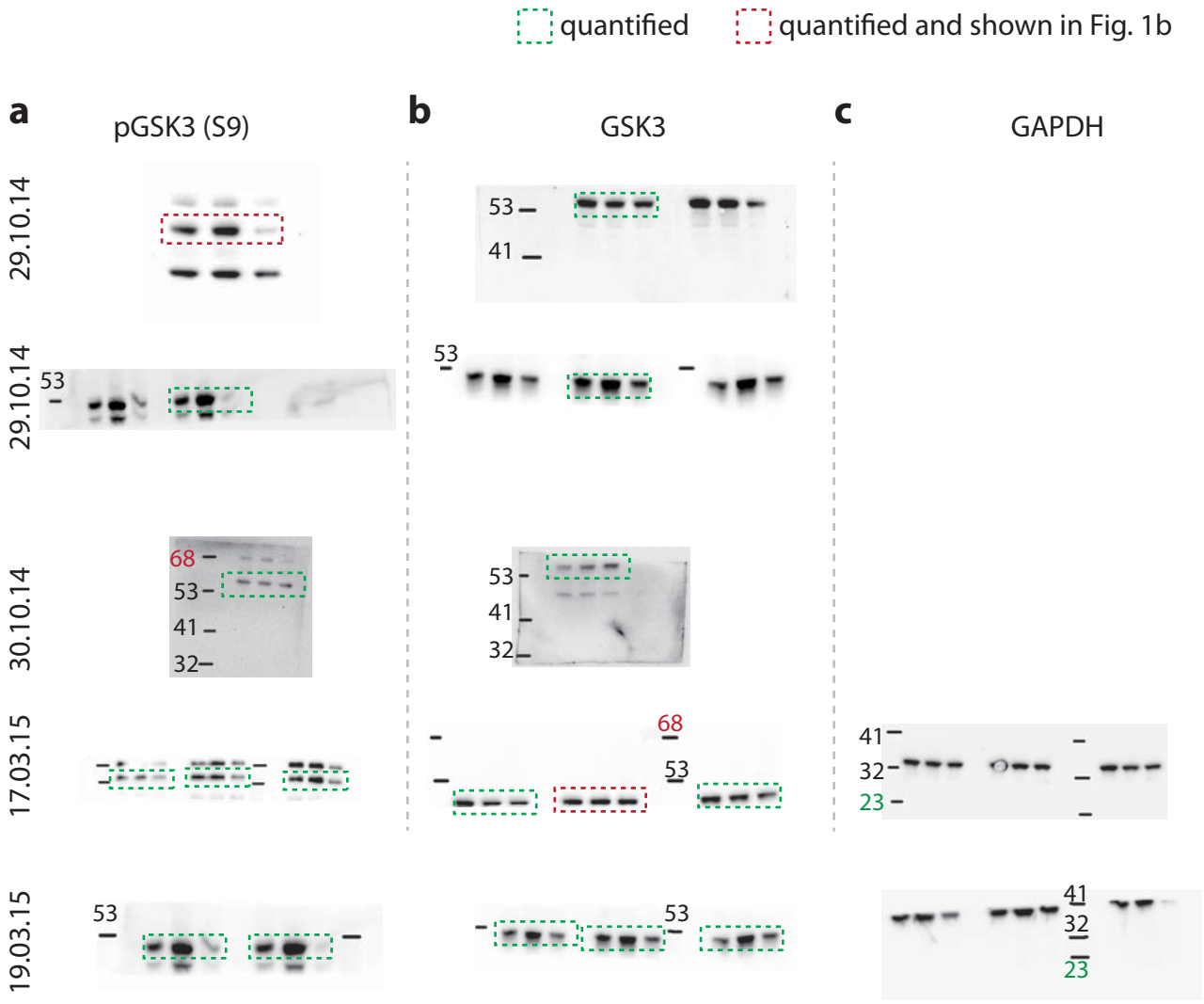
quantified
quantified and shown in Fig. 1b
a
pGSK3 (S9)
b
GSK3
c
GAPDH
29.10.14
29.10.14
30.10.14
17.03.15
19.03.15
53
68
41
32
23

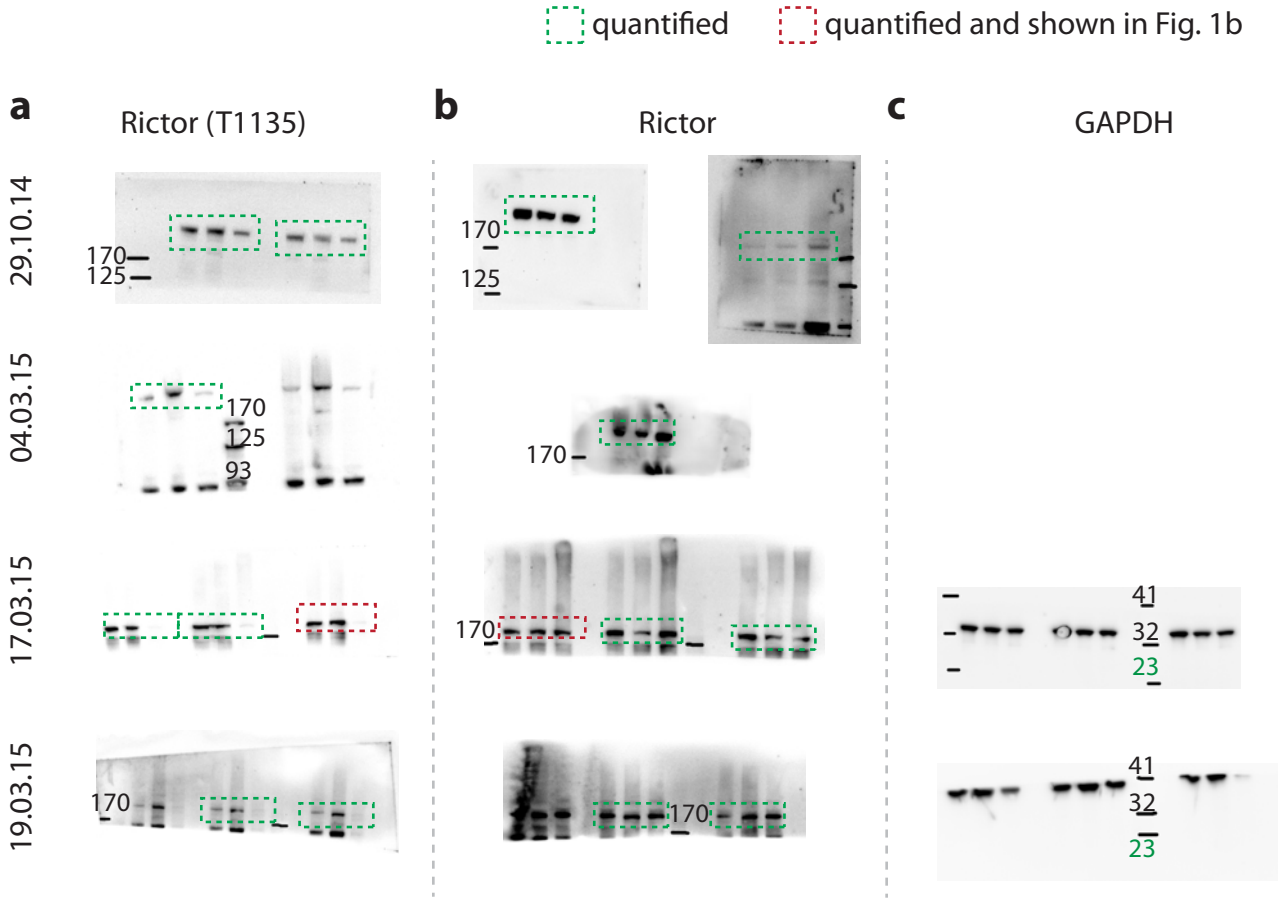
quantified
quantified and shown in Fig. 1b
a
Rictor (T1135)
b
Rictor
c
GAPDH
29.10.14
04.03.15
17.03.15
19.03.15
170
125
93
41
32
23

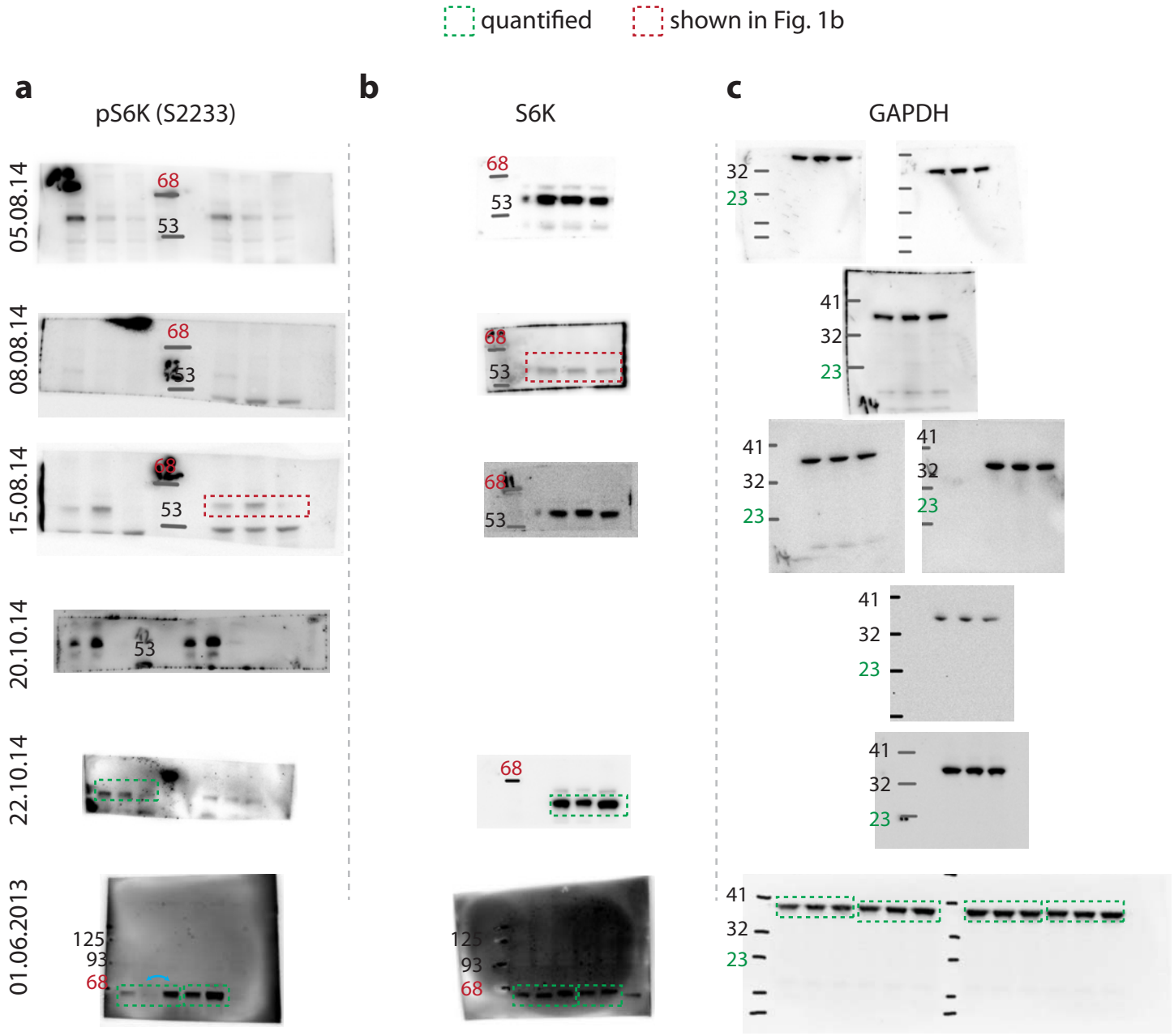
quantified
shown in Fig. 1b
a
pS6K (S2233)
b
S6K
c
GAPDH
05.08.14
08.08.14
15.08.14
20.10.14
22.10.14
01.06.2013
68
53
125
93
41
32
23

shown in Fig. 4d

PKCα-pS657

Akt-pT308

PKCα

Akt

pS PKC substrate

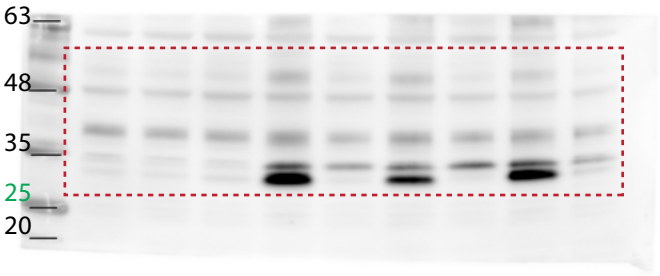

GSK3β-pS9

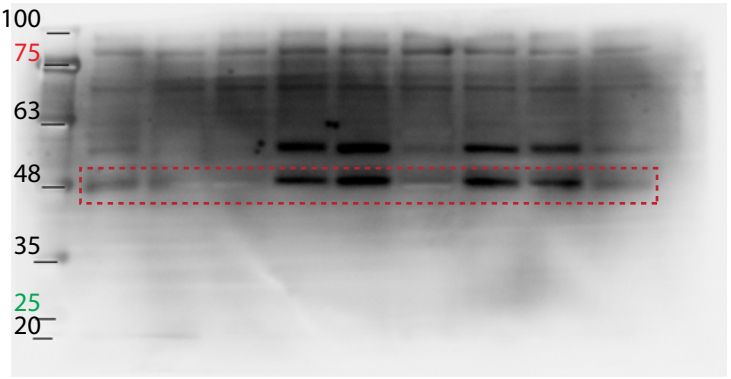

GAPDH

GSK3β

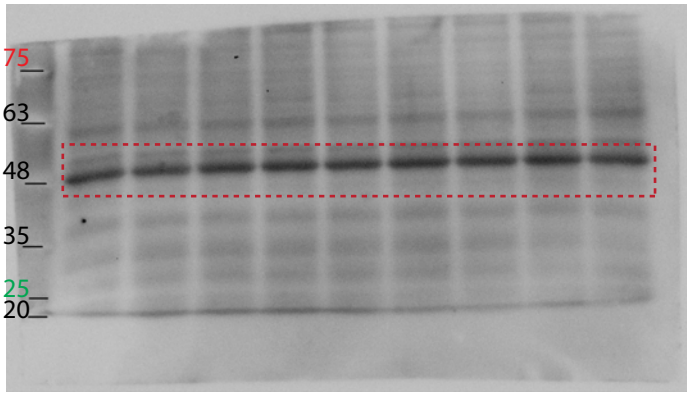

FLNc

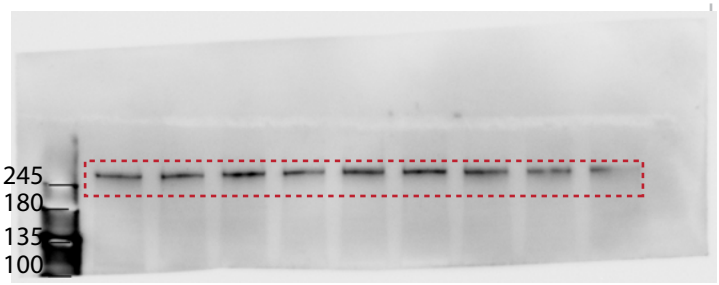

FLNc-pS2234

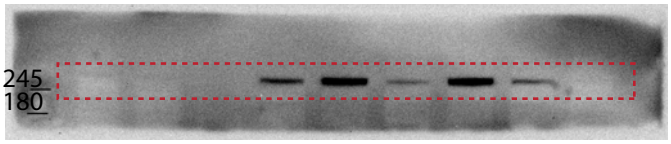

shown in Fig. 5e

His

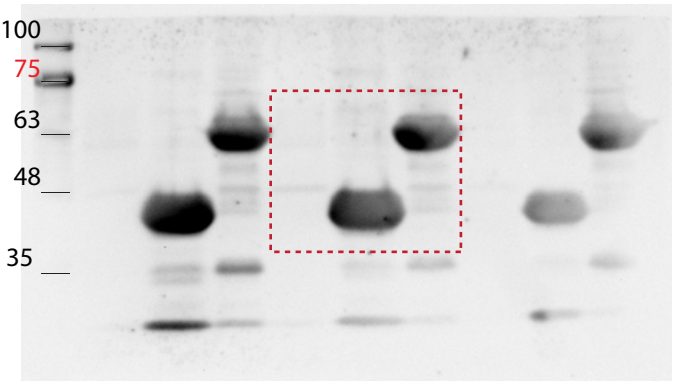

FILIP1

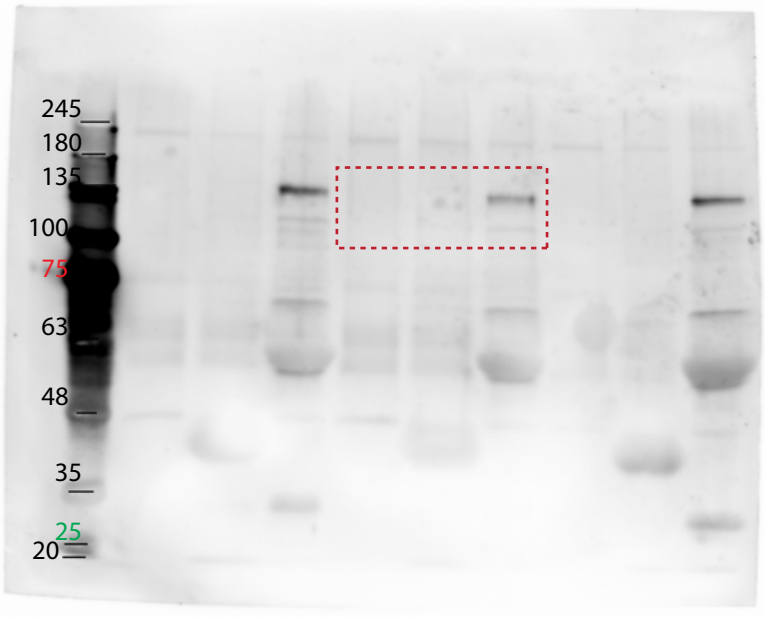

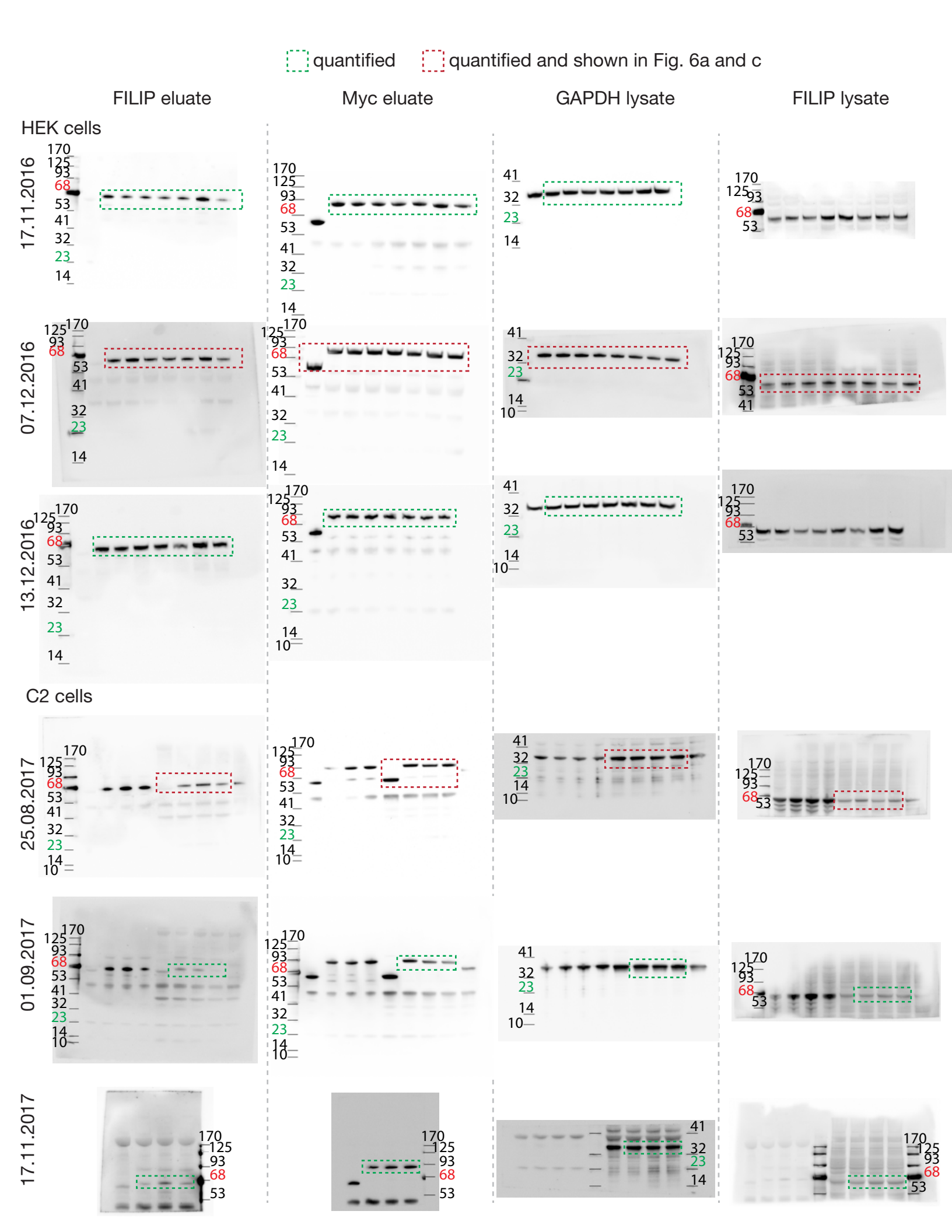
quantified
quantified and shown in Fig. 6a and c
FILIP eluate
Myc eluate
GAPDH lysate
FILIP lysate
HEK cells
17.11.2016
07.12.2016
13.12.2016
C2 cells
25.08.2017
01.09.2017
17.11.2017

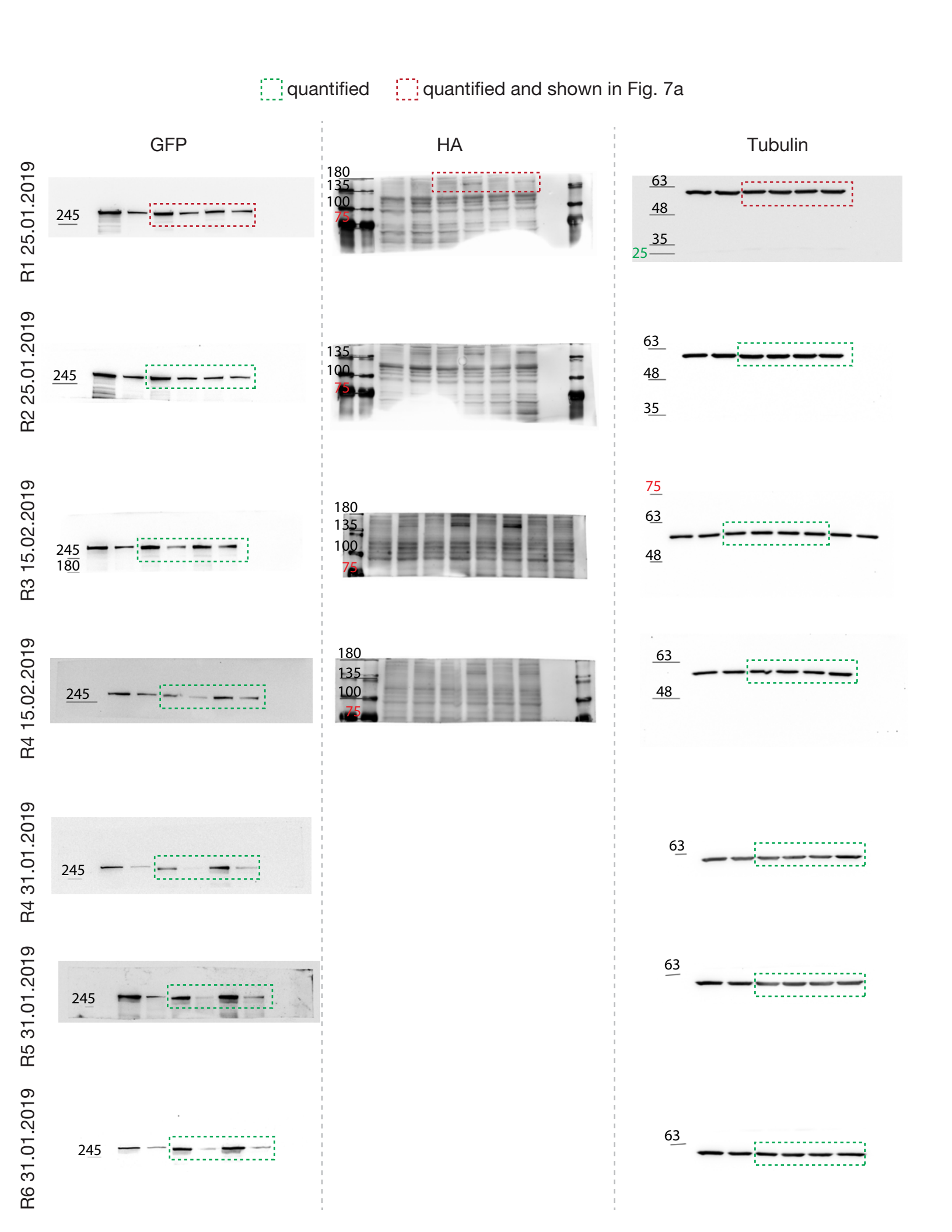
quantified
quantified and shown in Fig. 7a
GFP
HA
Tubulin
R1 25.01.2019
R2 25.01.2019
R3 15.02.2019
R4 15.02.2019
R4 31.01.2019
R5 31.01.2019
R6 31.01.2019
245
180
135
100
75
63
48
35
25

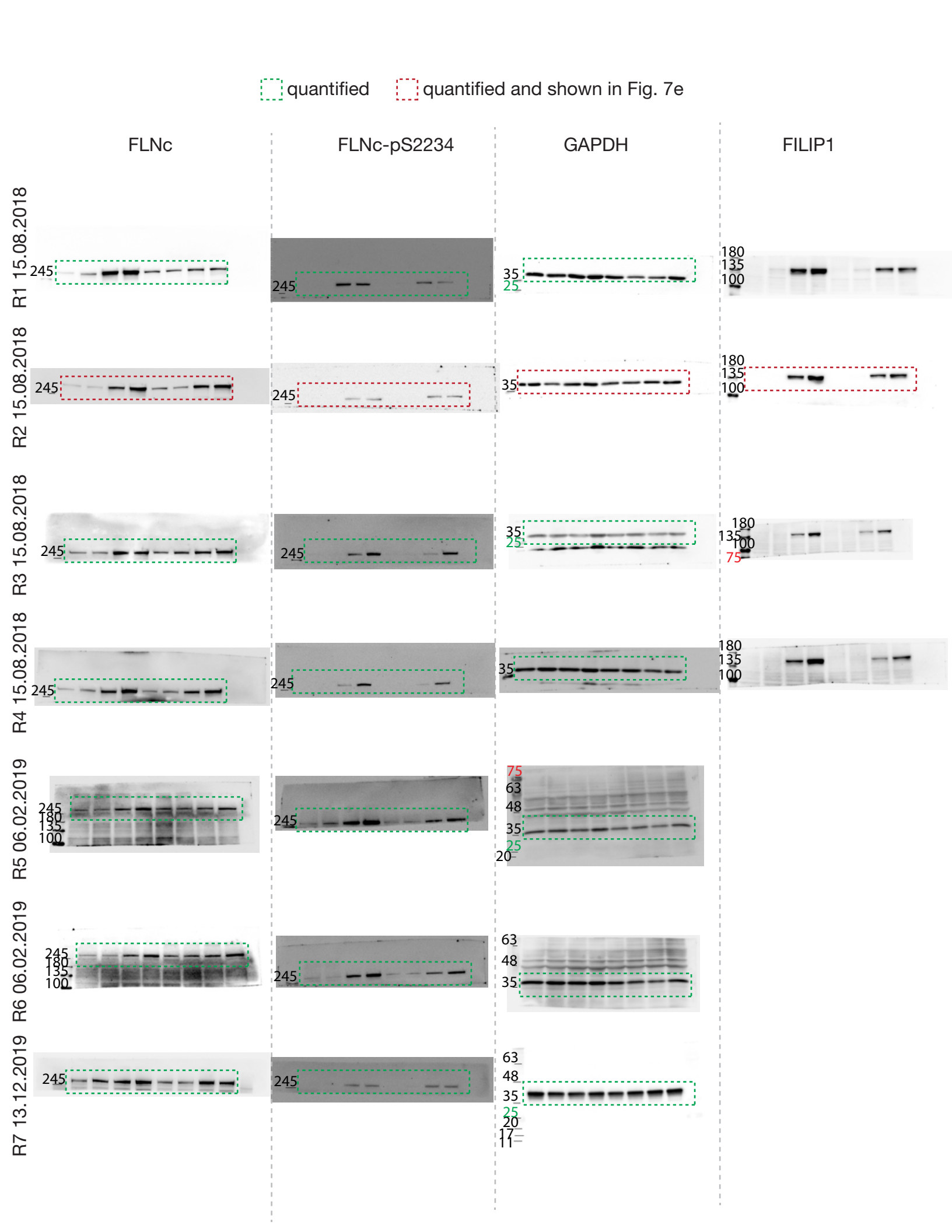
quantified
quantified and shown in Fig. 7e
FLNc
FLNc-pS2234
GAPDH
FILIP1
R1 15.08.2018
R2 15.08.2018
R3 15.08.2018
R4 15.08.2018
R5 06.02.2019
R6 06.02.2019
R7 13.12.2019
245
180
135
100
75
63
48
35
25
20
17
11

quantified and shown in Fig. 7h and Fig. S13

Eluates

Myc

Bag3

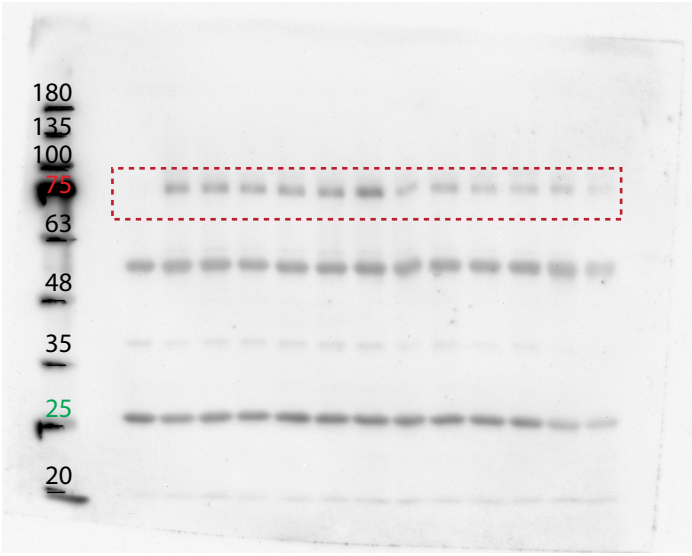

Ubiquitin

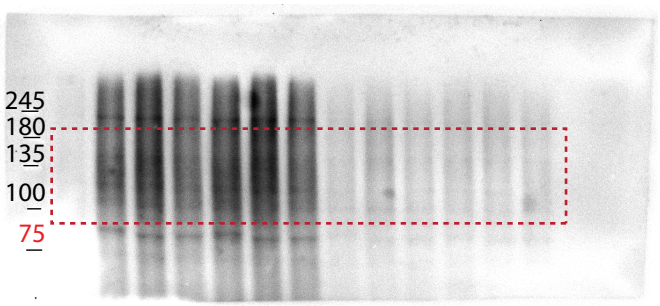

Lysates

HA

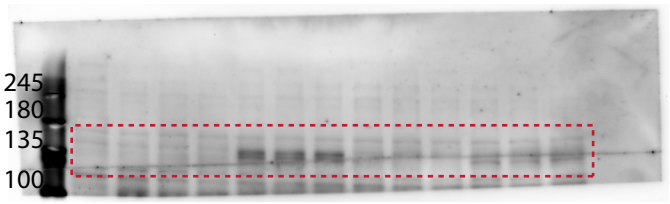

Myc

Tubulin

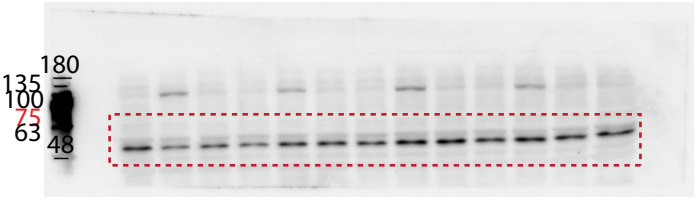

Bag3

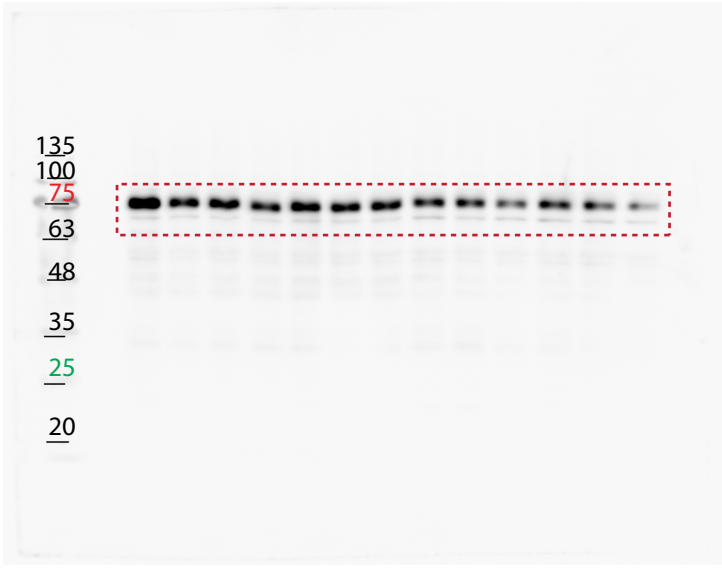

LC3

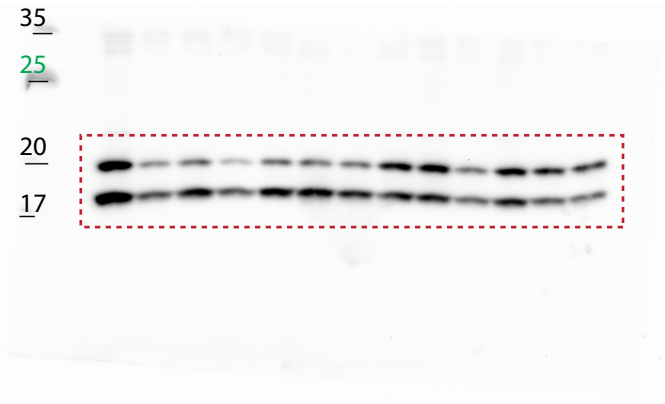

R1 20.11.2019

quantified in Fig. 7h

Myc

Ubiquitin

R2 14.12.2019

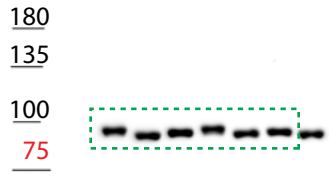

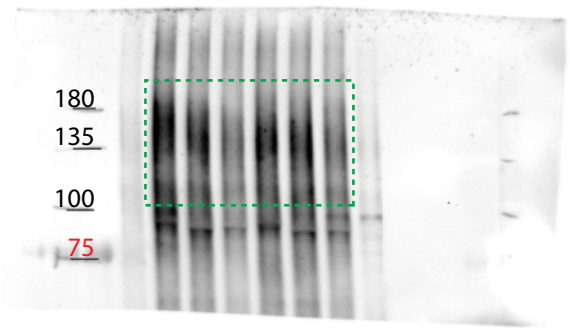

R3 14.12.2019

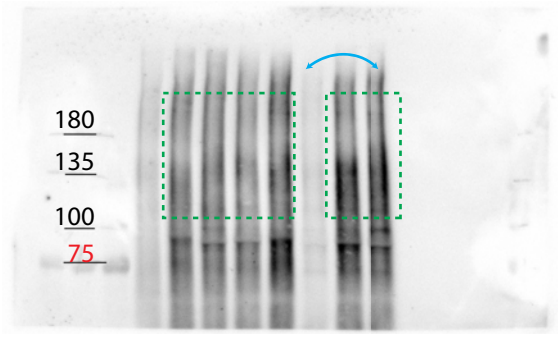

R4 14.12.2019

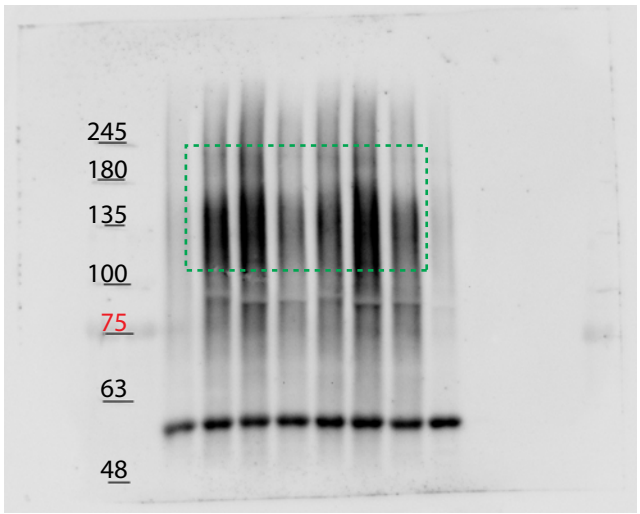

R5 05.02.2020

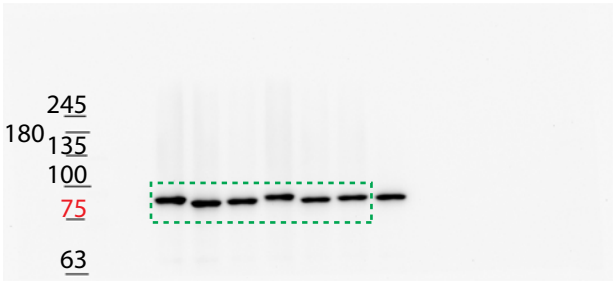

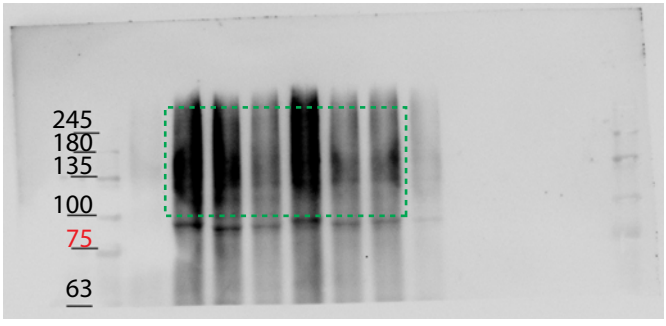

shown in Supplementary Fig. 1a

Akt

Akt-pT308

Akt-pS473

eEF2

eEF2-pT56

GAPDH

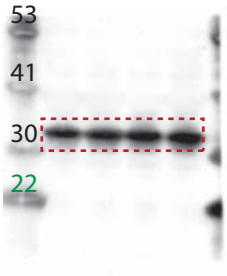

shown in Supplementary Fig. 4a

Akt-pS473

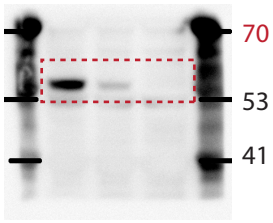

Akt-pT308

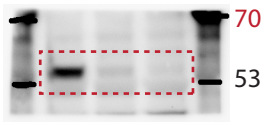

Akt

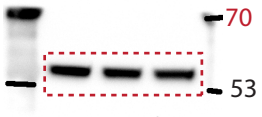

eEF-pT56

eEF

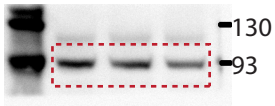

GSK3β-S9

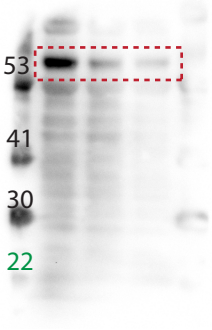

GSK3β

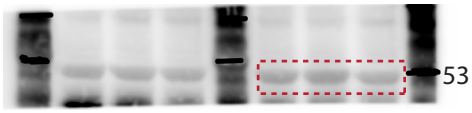

Rictor-pT1135

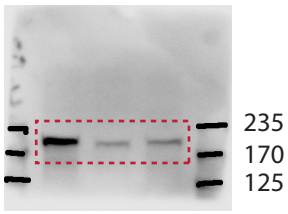

Rictor

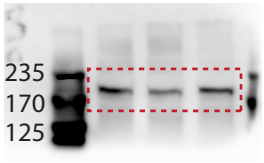

p44 MAPK-pY204
p42 MAPK-pT202

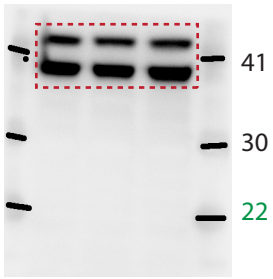

p44 MAPK
p42 MAPK

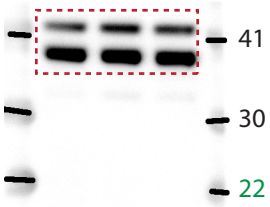

PKCα-pS657

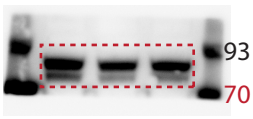

PKCα

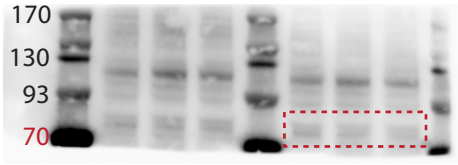

p70 S6K-pT389

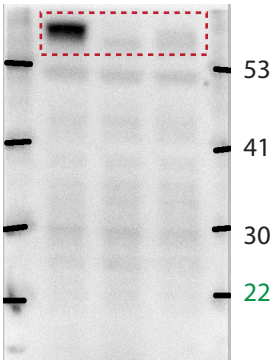

p70 S6K

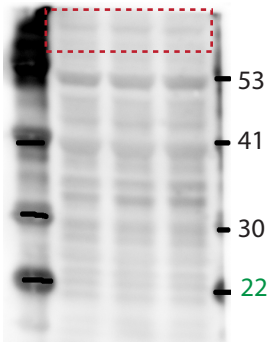

GAPDH

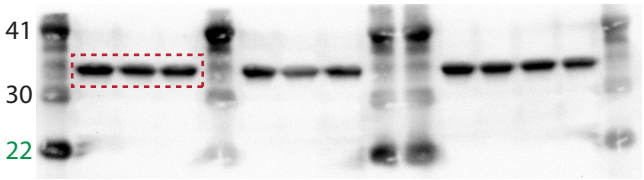

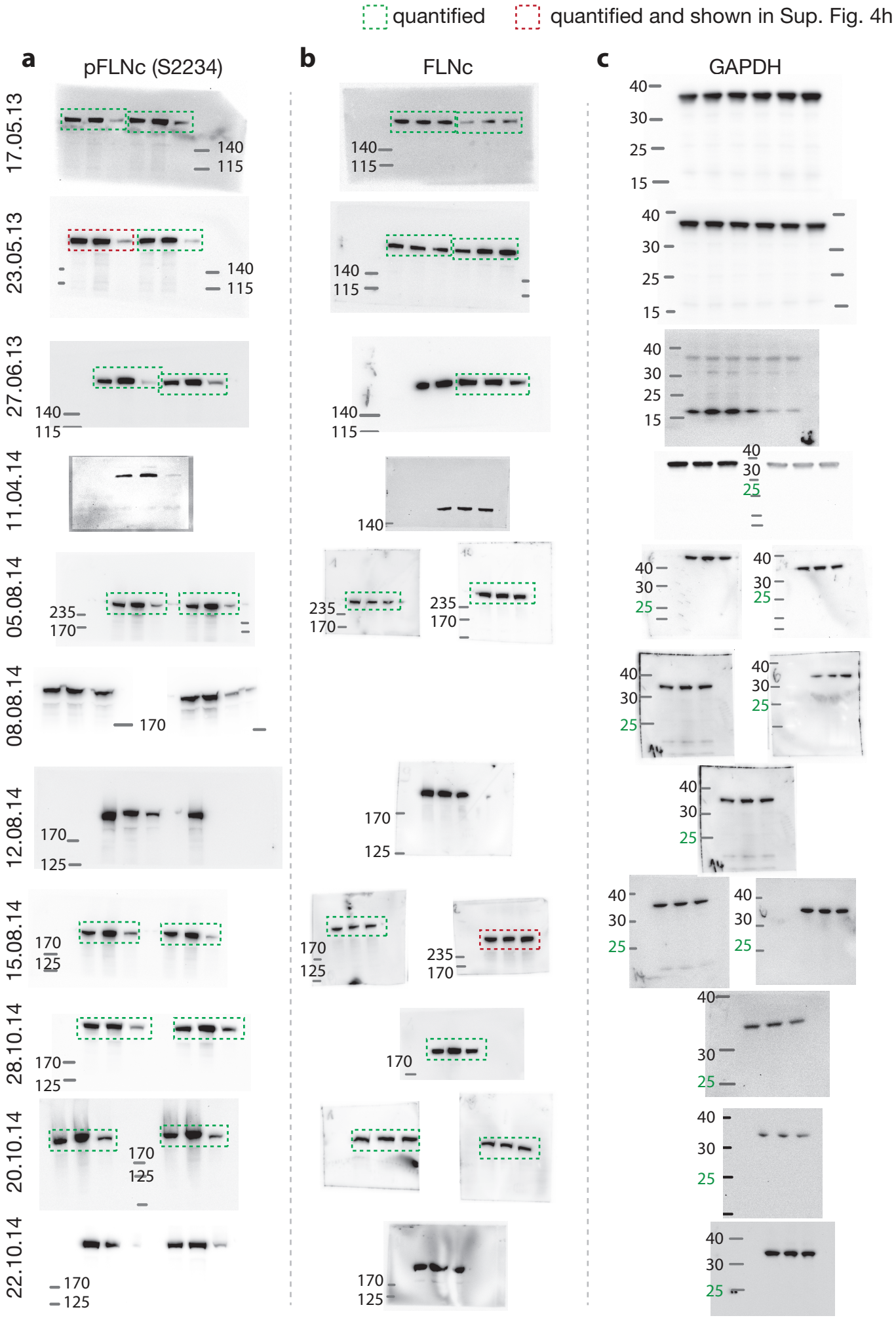
quantified
quantified and shown in Sup. Fig. 4h
a
pFLNc (S2234)
b
FLNc
c
GAPDH
17.05.13
23.05.13
27.06.13
11.04.14
05.08.14
08.08.14
12.08.14
15.08.14
28.10.14
20.10.14
22.10.14
140
115
235
170
125
40
30
25
15

shown in Supplementary Fig. 6b

FLNc-pS2233

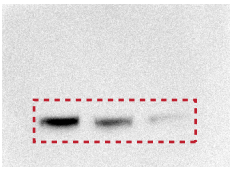

FLNc d16-20

GAPDH

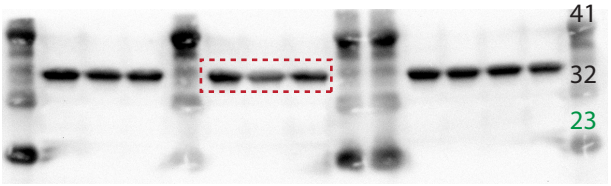

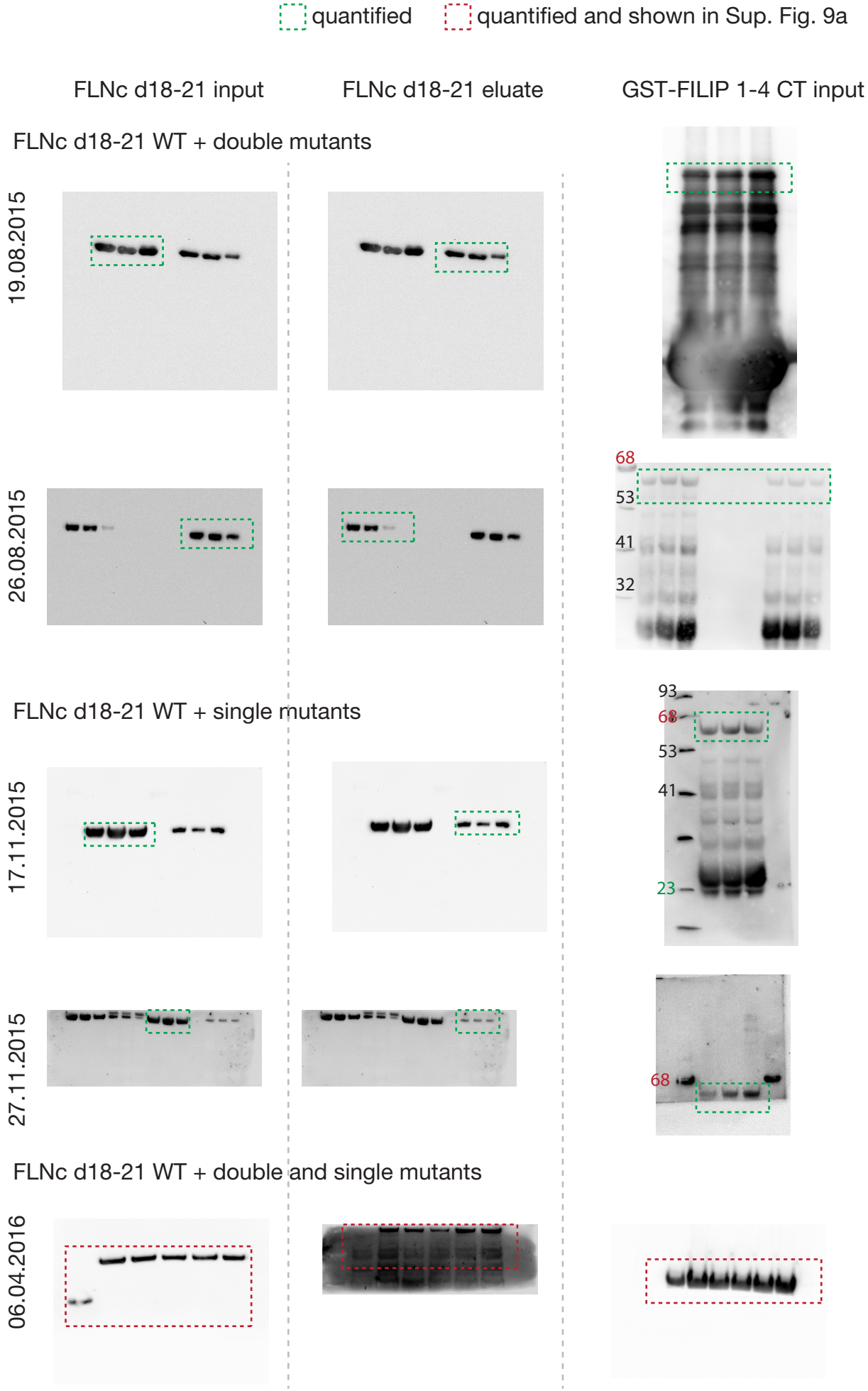

Supplementary Figure 2. Uncropped images of Western blots, shown in Fig. 1b, 4d, 5e, 6c, 6e, 7a, 7e, 7h/S13h, S1a, S4a, S4h, S6b and S9a.

Supplementary Figure 3

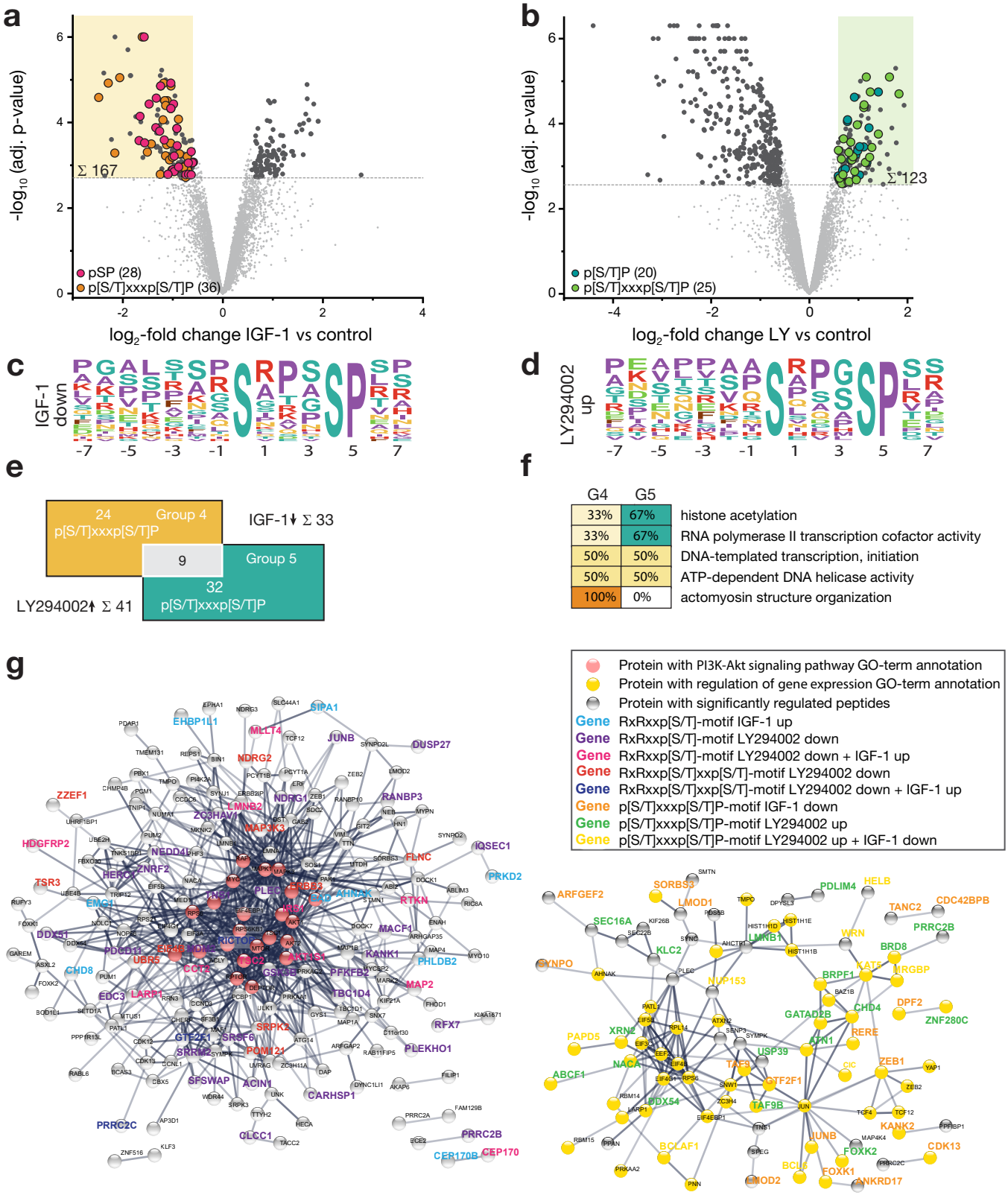

Supplementary Figure 3. Sequence motif analysis for proteins with phosphosites downregulated in response to PI3K/Akt/mTOR pathway activation or upregulated following inhibition. **a, b.** Volcano plots of phosphopeptides with localized phosphosites quantified in contracting C2 myotubes following IGF-1 (a) or LY294002 (b) treatment. Log_2-transformed mean SILAC ratios (control/treatment) were plotted against $-log_{10}$ adjusted p-values. Phosphopeptides with a minimum fold change of 1.5 and a FDR lower than 0.05 (n=3 independent experiments; moderated two-tailed student's t-test) are shown as larger dark gray circles. Among these, phosphopeptides are color-coded according to their phosphorylation sequence motif as indicated and regions of interest are highlighted in each plot. **c, d.** Motif-X analysis of regulated phosphopeptides. The proline-directed motif pSxxxSP was 30-fold and and 26-fold enriched following treatment with IGF-1 (c) and LY294002 (d), respectively. x, any amino acid. **e.** Overlap of unique phosphopeptides comprising the proline-directed motif p[S/T]xxxp[S/T]P in Group 4 (IGF-1 downregulated) and Group 5 (LY294002 upregulated). **f.** Combined GO enrichment analysis of phosphopeptides in group 4 and 5 (G4, G5) shown in (e). GO analysis was performed with the Cytoscape app ClueGO using Benjamini-Hochberg correction for p-value calculation. Only pathways with a p-value ≤ 0.05 were considered to be enriched. **g.** STRING network analysis of proteins with regulated phosphopeptides (fold-change ≥ 1.5; FDR < 0.05; n=3; moderated two-tailed student's t-test) following treatment of C2 myotubes with LY294002 or IGF-1. Proteins annotated as components of the PI3K/Akt pathway are highlighted by red bullets, proteins annotated with the GO term "gene expression" by yellow bullets. Gene names of proteins comprising a regulated phosphorylation site within a short or extended basophilic motif or the p[S/T]xxxp[S/T]P motif are color-coded as indicated.

Supplementary Figure 4

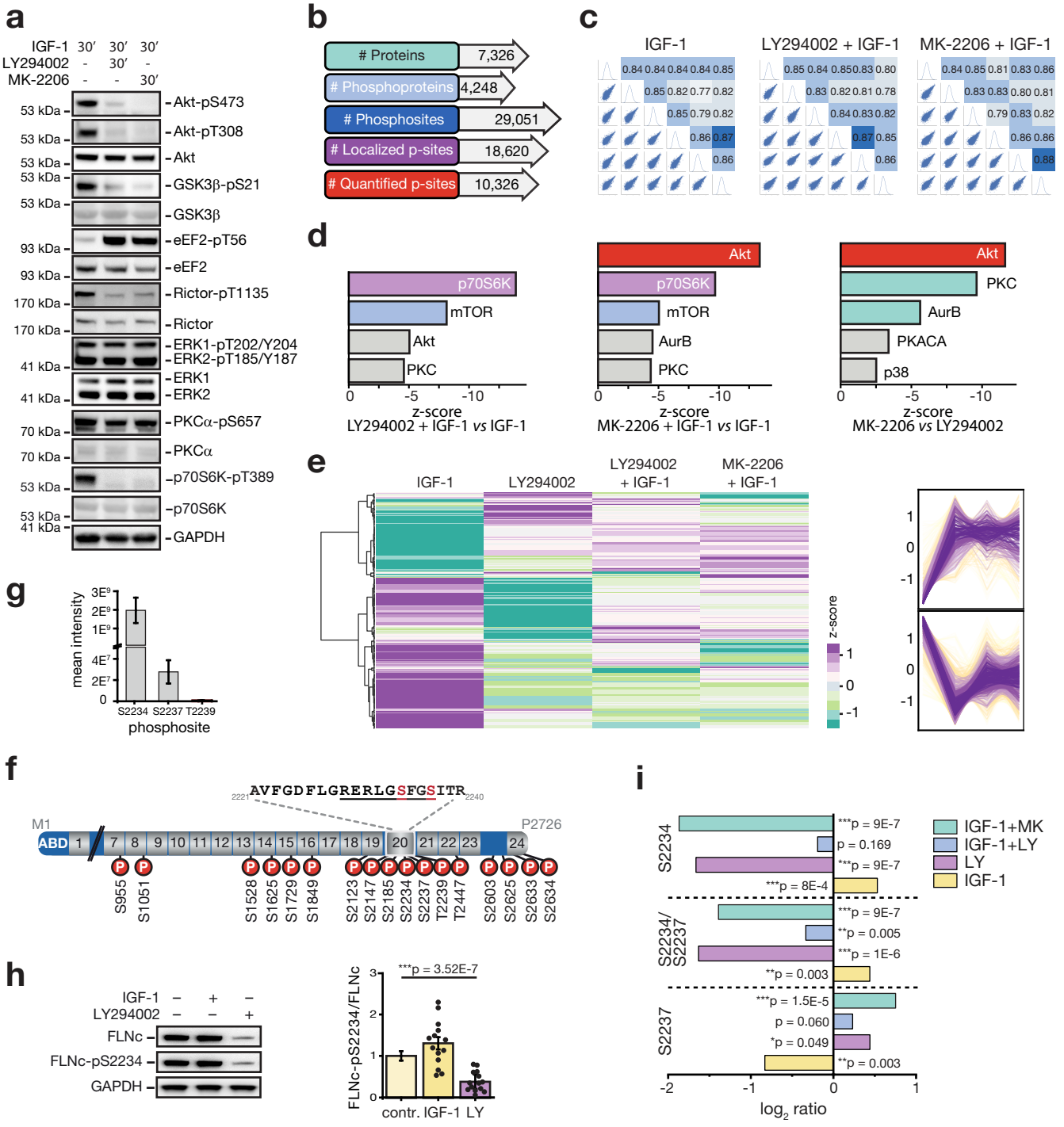

Supplementary Figure 4. Study of the PI3K/Akt/mTOR signaling landscape in contracting C2 myotubes using LY294002 (LY) and MK-2206 (MK). **a.** Contracting C2 myotubes, differentially labeled by SILAC amino acids, were treated for 30 min with IGF-1 in combination with LY or MK as indicated. Immunoblot analysis of PI3K/Akt/mTOR pathway activity using phospho-specific antibodies against established readouts. **b.** Overview of the number of identified proteins and phospho-proteins as well as the number of counted, localized (≥ 0.75) as well as localized and reproducibly quantified phosphosites in 3 out of 6 independent experiments obtained by quantitative MS-based phosphoproteome analysis and MaxQuant data analysis together with the IGF-1/LY data. **c.** Pearson correlation analysis of the phosphoproteomic data for the three different treatments (IGF-1, IGF-1+LY, IGF-1+MK, n=6). **d.** Z-score for the top down-regulated kinases based on kinase-substrate enrichment analysis (KSEA) for the different treatments as indicated. **e.** Hierarchical cluster analysis of all peptides that were significantly regulated in at least one of the four treatments (fold-change > ±1.5, adjusted p-value < 0.05 for IGF-1/LY dataset and < 0.01 for the LY/MK dataset) in the combined analysis (left panel). Two main cluster were obtained, the upper with 317 phosphopeptides, the lower with 560 phosphopeptides (right panel) **f.** Phosphosites of endogenous FLNc from mouse skeletal myotubes identified and quantified in this study. pS2234 and pS2237 are located in the extended basophilic motif RxRxxpSxxpS within the conserved Ig-like domain 20 of FLNc. **g.** Mean intensities of FLNc phosphopeptides with pS2234, pS2237 or pS2239 (n=3 independent experiments, SEM) **h.** Immunoblot analysis and quantification of signals detected for endogenous FLNc-pS2234 in comparison to total FLNc following treatment of mouse skeletal myotubes with IGF-1 or LY. Shown are normalized values from 14 replicates ± SEM. A paired two-tailed student's t-test was performed. **i.** FLNc phosphopeptides with the sequence 2232-LGSFGSITR-2240, either singly or doubly phosphorylated at S2234 and S2237, were regulated in abundance following activation (IGF-1) or inhibition (LY, IGF-1+MK, IGF-1+LY) of PI3K/Akt signaling. Shown are the $\log_2$ ratios and adjusted p-values calculated for each of the phosphosites.

Supplementary Figure 5

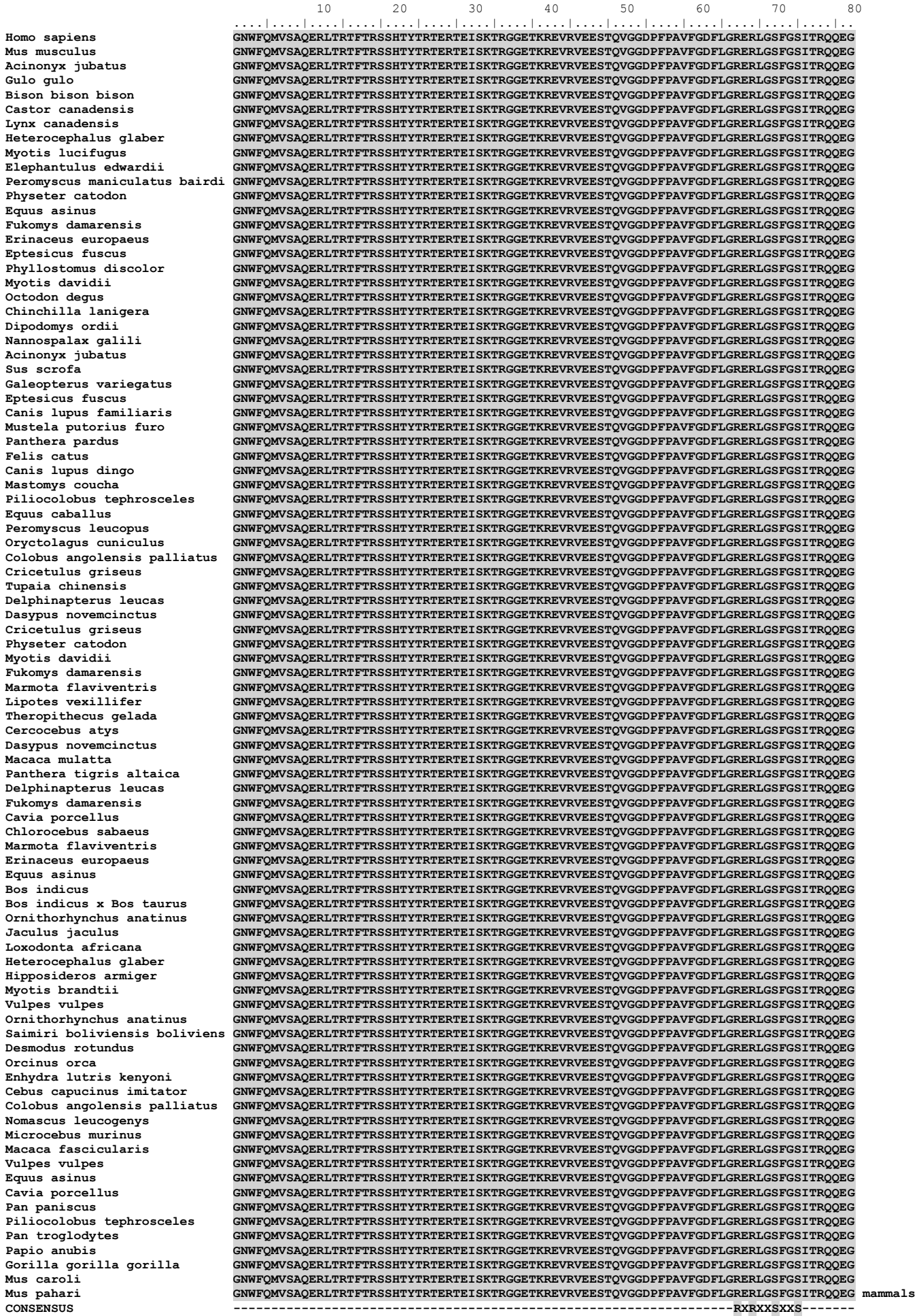

Supplementary Figure 5. Sequence alignment across mammalian species of the FLNc specific insertion in domain 20, comprising 82 amino acids.

Supplementary Figure 6

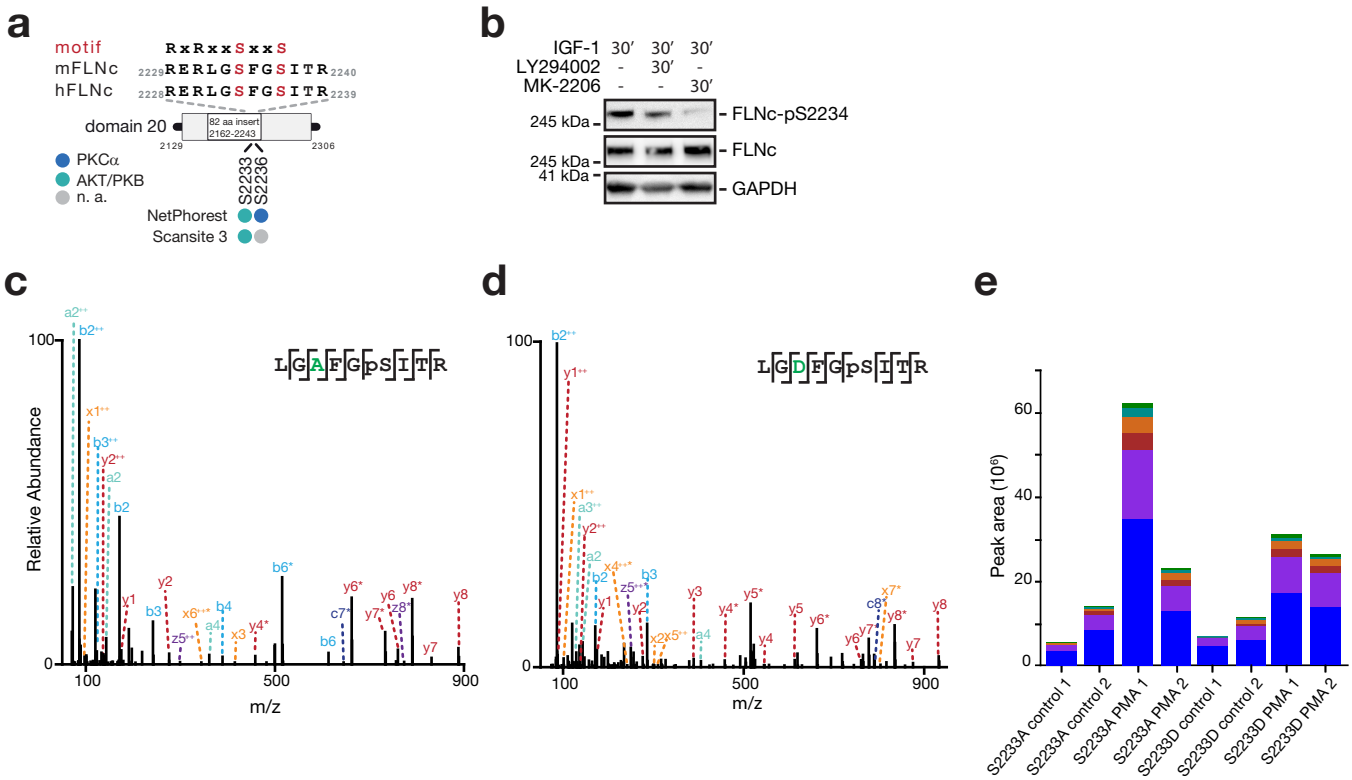

Supplementary Figure 6. Analysis of phosphorylation status of endogenous mouse (m) FLNc as well as human (h) FLNc d18-21 S2233D and S2233A mutants. **a.** Kinase prediction for pS2233 and pS2236 of mFLNc and hFLNc using the algorithms NetPhorest and Scansite 3. Both phosphosites are part of the extended basophilic motif located in the unique 82-amino acid insert in domain 20, which is highly conserved in mammals. **b.** Immunoblot analysis of mFLNc phosphorylation at S2234 in C2 myotubes in dependency of MK-2206 and LY294002 inhibition in combination IGF-1 as indicated. **c, d.** C2 cells expressing hFLNc d18-21 in which S2233 was mutated to alanine (A) or aspartate (D) were treated with PMA for activation of PKC followed by phosphopeptide analysis in a targeted MS approach using higher collisional dissociation (HCD) as outlined in Figure 4c. HCD spectrum of the phosphopeptide (a) LGAFGpSITR from the FLNc d18-21 S2233A mutant and (b) LGDFGpSITR from the FLNc d18-21 S2233D mutant. The site-exchanged amino acids (S to A, S to D) are highlighted in green. **e.** Precursor and transition areas determined by Skyline analysis of the targeted MS data obtained for the phosphopeptides shown in (c) and (d).

Supplementary Figure 7

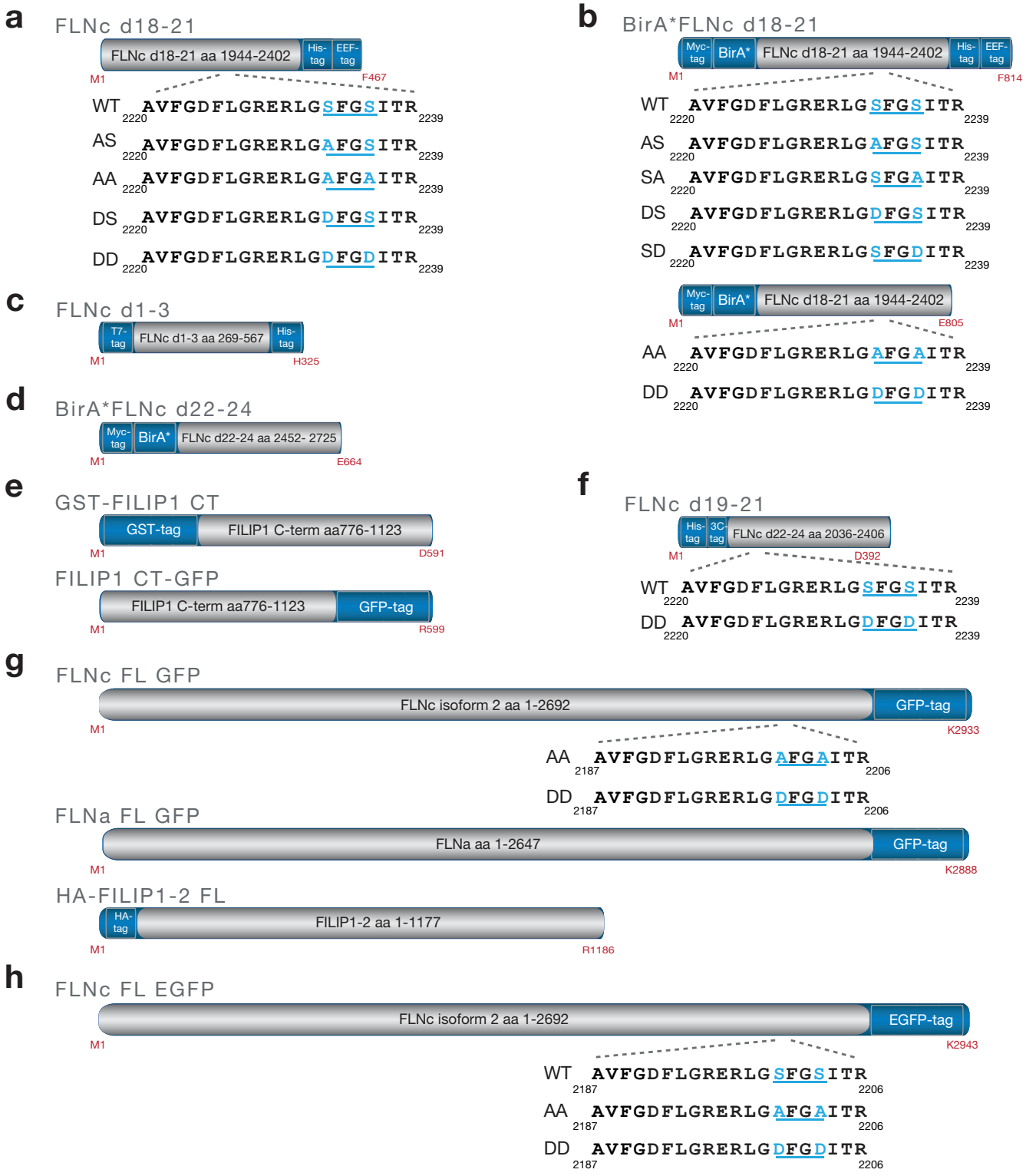

Supplementary Figure 7. FLNc phosphosite mutants and fusion proteins used in this work. **a.** Schematic illustration of human FLNc d18-21 constructs used for bacterial transformations comprising a 6xHis tag and an EEF tag fused to the carboxy-terminus. Phosphosite mutants were generated from the respective wild-type construct by exchange of one or two serines (S) to alanine (A) or aspartate (D) as indicated. WT, wild-type; d, domain **b.** Schematic illustration of human FLNc d18-21 constructs used for transfections of mammalian cells comprising a Myc-tag and a BirA* sequence fused to the amino-terminus. Additionally, wild-type and single site mutants contain a 6xHis tag and an EEF tag fused to the carboxy-terminus. Phosphosite mutants were generated as described in (a). BirA*, promiscuous biotin ligase. **c.** Schematic illustration of human FLNc d1-3 construct used for bacterial transformations comprising a T7 tag and a 6xHis tag fused to the amino- and carboxy-terminus, respectively. **d.** Schematic illustration of human FLNc d22-24 construct used for transfections of mammalian cells comprising a Myc-tag and a BirA* sequence fused to the amino-terminus. **e.** Schematic illustration of FILIP1 carboxy-terminal constructs. For transformation of bacterial cells, the construct was fused to GST at its amino-terminus. For transfection of mammalian cells, the construct was fused to GFP at its carboxy-terminus. CT, carboxy-terminus. **f.** Schematic illustration of the phosphomimicking human FLNc d19-21 construct used for fluorescence correlation spectroscopy analysis comprising a 6xHis tag fused to the amino-terminus. The phosphomimicking mutant was generated from the respective wild-type construct by exchange of two serine residues (SS) to aspartate (DD) as indicated. WT, wild-type. **g.** Schematic illustration of constructs used for co-expression of FLNa, FLNc and FILIP1. FLNa and FLNc full-length constructs were fused to GFP at its carboxy-terminus. FLNc double phosphosite mutants were generated from the respective WT construct by exchange of two serine residues (SS) to alanine (AA) or aspartate (DD) as indicated. FILIP1-2 was fused to an HA-tag at its amino-terminus. FL, full-length. **h.** Schematic illustration of FLNc constructs used for fluorescence recovery after photobleach fused to a carboxy-terminal EGFP. Phosphomimicking mutants were generated from the respective wild-type construct by exchange of two serine residues (SS) to aspartate (DD) or alanine (AA) as indicated. FL, full length. WT, wild-type.

Supplementary Figure 8

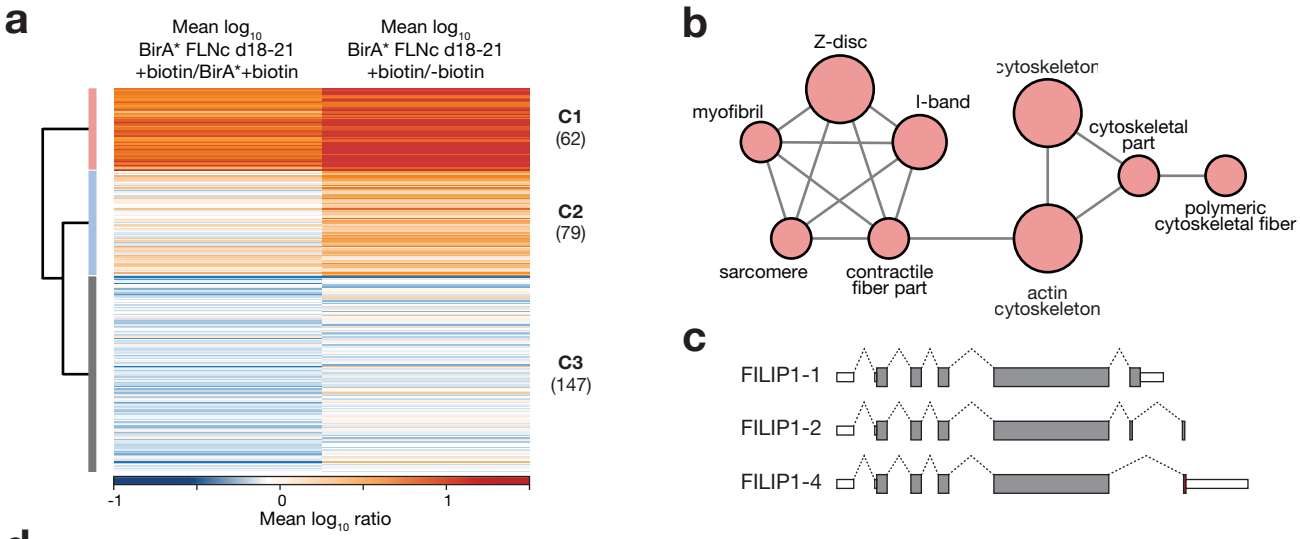

d

```
Q7Z7B0     FILIP1-1  1121   GASKVTSTITITPVTTSSARGTQSV---SGQDGSSQRPTPTRIPMSKGMKAGKPVVAAPGAGNLTKFEPRAETQSMKIELKKSAASSTTSLGGGKG   1213
Q7Z7B0-2   FILIP1-2  1121   GASKVTSTITITPVTTSSARGTQSV---SGQDGSSQRPTPTRIPMSK---ESIIIHQLRMNSR                                  1177
Q7Z7B0-3   FILIP1-3  873    GASKVTSTITITPVTTSSARGTQSV---SGQDGSSQRPTPTRIPMSKGMKAGKPVVAAPGAGNLTKFEPRAETQSMKIELKKSAASSTTSLGGGKG    965
Novel      FILIP1-4  1121   GASKVTSTITITPVTTSSARGTQSV---KASSFTSYE                                                              1154
```

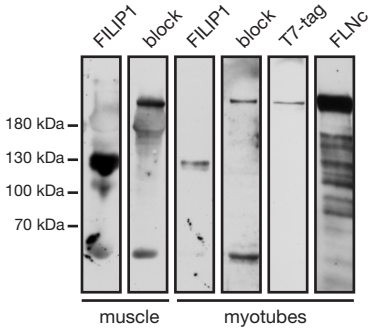

f

FLNc domains	lacZ	His3
d16-19	+	+++
d16-17	-	+
d17-19	+++	+++
d18-21	+++	+++
d18-19	-	-
d20-21	++	++

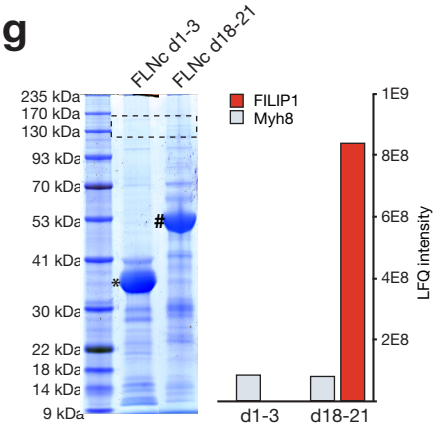

h

FLNC_MOUSE Isoform 2 of Filamin-C Q8VHX6-2
Protein sequence coverage: 78%

```
1     MMNNSNYSDA SGLGLVDEAD EMPSTEKDLA EDAPWKKIQQ NTFTRWCNEH LKCVGKRLTD LQRDLSDGLR LIALLEVLSQ KRMYRKFHPR PNFRQMKLEN
101   VSVALEFLER EHIKLVSIDS KAIVDGNLKL ILGLIWTLIL HYSISMPMWE DEDDEDARKQ TPKQRLLGWI QNKVPQLPIT NFNRDWQDGK ALGALVDNCA
201   PGLCPDWEAW DPNQPVQNAR EAMQQADDWL GVPQVIAPEE IVDPNVDEHS VMTYLSQFPK AKLKPGAPVR SKQLNPKKAI AYGPGIEPQG NTVLQPAHFT
301   VQTVDAGVGE VLVYIEDPEG HTEEAKVVPN NDKDRTYAVS YVPKVAGLHK VTVLFAGQNI ERSPFEVNVG MALGDANKVS ARGPGLEPVG NVANKPTYFD
401   IYTAGAGTGD VAVVIVDPQG RRDTVEVALE DKGDNTFRCT YRPVMEGPHT VHVAFAGAPI TRSPFPVHVA EACNPNACRA SGRGLQPKGV RVKEVADFKV
501   FTKGAGSGEL KVTVKGPKGT EEPVKVREAG DGVFECEYYP VVPGKYVVTI TWGGYAIPRS PFEVQVSPEA GAQKVRAWGP GLETGQVGKS ADFVVEAIGT
601   EVGTLGFSIE GPSQAKIECD DKGDGSCDVR YWPTEPGEYA VHVICDDEDI RDSPFIAHIQ PAPPDCFPDK VKAFGPGLEP TGCIVDRPAE FTIDARAAGK
701   GDLKLYAQDA DGCPIDIKVI PNGDGTFRCS YVPTKPIKHT IIVSWGGVNV PKSPFRVNVG EGSHPERVKV YGPGVEKTGL KANEPTYFTV DCSEAGQGDV
801   SIGIKCAPGV VGPVEADIDF DIIKNDNDTF TVKYTPPGAG HYTIMVLFAN QEIPASPFHI KVDPSHDASK VKAEGPGLSR TGVEVGKPTH FTVLTKGAGK
901   AKLDVHFAGA AKGEAVRDFE IIDNHDYSYT VKYTAVQQGN MAVTVTYGGD PVPKSPFVVN VAPPLDLSKV KVQGLNSKVA VGQEQAFSVN TRGAGGQGQL
1001  DVRMTSPSRR PIPCKLEPGG GAEAQAVRYM PPEEGPYKVD ITYDGHPVPG SPFAVEGVLP PDPSKVCAYG PGLKGGLVGT PAPFSIDTKG AGTGGLGLTV
1101  EGPCEAKIEC QDNGDGSCAV SYLPTEPGEY TINILFAEAH IPGSPFKATI QPVFDPSKVR ASGPGLERGK AGEAATFTVD CSEAGEAELT IEILSDAGVK
1201  AEVLIQNNAD GTYHITYSPA FPGTYTITIK YGGHPIPKFP TRVHVQPAVD TSGIKVSGPG VEPHGVLREV TTEFTVDARS LTATGGNHVT ARVLNPSGAK
1301  TDTYVTDNGD GTYRVQYTAY EEGVHLVEVL YDEVAVPKSP FRVGVTEGCD PTRVRAFGPG LEGGLVNKAN RFTVETRGAG TGGLGLAIEG PSEAKMSCKD
1401  NKDGSCTVEY IPFTPGDYDV NITFGGQPIP GSPFRVPVKD VVDPGKVKCS GPGLGTGVRA RVPQTFTVDC SQAGRAPLQV AVLGPTGVAE PVEVRDNGDG
1501  THTVHYTPAT DGPYTVAVKY ADQEVPRSPF KIKVLPSHDA SKVRASGPGL NASGIPASLP VEFTIDARDA GQGLLTVQIL DPEGKPKKAN IRDNGDGTYT
1601  VSYLPDMSGR YTITIKYGGD EIPYSPFRIH ALPTGDASKC LVTVSIGGHG LGACLGPRIQ IGEETVITVD AKAAGKGKVT CTVSTPDGAE LDVDVVENHD
1701  GTFDIYYTAP EPGKYVITIR FGGEHIPNSP FHVLATEEPV VPVEPLESML RPFNLVIPFT VQKGELTGEV RMPSGKTARP NITDNKDGTI TVRYAPTEKG
1801  LHQMGIKYDG NHIPGSPLQF YVDAINSRHV SAYGPGLSHG MVNKPATFTI VTKDAGEGGL SLAVEGPSKA EITCKDNKDG TCTVSYLPTA PGDYSIIVRF
1901  DDKHIPGSPF TAKITGDDSM RTSQLNVGTS TDVSLKITEG DLSQLTASIR APSGNEEPCL LKRLPNRHIG ISFTPKEVGE HVVSVRKSGK HVTNSPFKIL
2001  VGPSEIGDAS KVRVWGKGLS EGQTFQVAEF IVDTRNAGYG GLGLSIEGPS KVDINCEDME DGTCKVTYCP TEPGTYIINI KFADKHVPGS PFTVKVTGEG
2101  RMKESITRRR QAPSIATIGS TCDLNLKIPG NWFQMVSAQE RLTRTFTRSS HTYTRTERTE ISKTRGGETK REVRVEESTQ VGGDPFPAVF GDFLGRERLG
2201  SFGSITRQQE GEASSQDMTA QVTSPSGKTE AAEIVEGEDS AYSVRFVPQE MGPHTVTVKY RGQHVPGSPF QFTVGPLGEG GAHKVRAGGT GLERGVAGVP
2301  AEFSIWTREA GAGGLSIAVE GPSKAEIAFE DRKDGSCGVS YVVQEPGDYE VSIKFNDEHI PDSPFVVPVA SLSDDARRLT VTSLQETGLK VNQPASFAVQ
2401  LNGARGVIDA RVHTPSGAVE ECYVSELDSD KHTIRFIPHE NGVHSIDVKF NGAHIPGSPF KIRVGEQSQA GDPGLVSAYG PGLEGGTTGV SSEFIVNTQN
2501  AGSGALSVTI DGPSKVQLDC RECPEGHVVT YTPMAPGNYL IAIKYGGPQH IVGSPFKAKV TGPRLSGGHS LHETSTVLVE TVTKSSSSRG ASYSSIPKFS
2601  SDASKVVTRG PGLSQAFVGQ KNSFTVDCSK AGTNMMMVGV HGPKTPCEEV YVKHMGNRVY NVTYTVKEKG DYILIVKWGD ESVPGSPFKV NVP
```

Supplementary Figure 8. Identification and validation of the interaction of FLNc and FILIP1. **a.** Hierarchical cluster analysis of the SILAC data obtained in the study of the protein nano-environment around hFLNc d18-21 by in vivo proximity labeling in skeletal myotubes. Mean $\log_{10}$ transformed SILAC ratios of quantified proteins were used (n=3 independent experiments). Only proteins in cluster 1 were deemed components of the hFLNc d18-21 interactome, since they were strongly enriched in comparison to both controls. Cluster 2 and 3 mainly contained unspecific binding partners and contaminants. Cluster 1, light red; cluster 2, light blue; cluster 3, gray. **b.** GO enrichment analysis. Shown are the cellular compartments containing proteins enriched in cluster 1. Z-disc and Z-disc-associated ontologies were overrepresented in cluster 1. **c.** Schematic illustration of FILIP1 isoforms. Shown are exons and slicing events. The isoforms FILIP1-1 and FILIP1-2 represent the Uniprot entries Q7Z7B0-1 and Q7Z7B0-2, respectively. The isoform FILIP1-4 lacks exon 6 as a result of alternative splicing. **d.** Sequence alignment of the carboxy-termini of FILIP1 isoforms 1 to 4 using Clustal Omega. **e.** Immunoblot analysis using an antiserum directed against its carboxy-terminus shows expression of FILIP1 (~130 kDa) in mouse skeletal muscle (lane 1) and cultured C2C12 myotubes (lane 3). The specificity of the antiserum was shown by adding the antigen (T7-tagged FILIP1-2 CT) to the antibody solution ("block", lanes 2 and 4). Binding to FILIP1 was abolished, but a distinct band above the 180 kDa marker band appeared, indicating binding of the antibody/antigen complex to another protein in the extracts. The presence of FILIP1-2 CT was confirmed using T7-tag antibody (lane 5), whereas binding of the antibody/antigen complex to endogenous FLNc was confirmed using anti-FLNc antibody (lane 6). **f.** Yeast-two hybrid analysis indicates binding of FILIP1-4 to FLNc d16-19, d17-19, d18-21 and d20-21 in yeast cells. -: no binding; +: weak binding; ++: moderate binding; +++: strong binding **g.** Coomassie-stained gel from FLNc d1-3 and FLNc d18-21 pulldown with myotube lysates. Bands of recombinant FLNc d1-3 (*) and recombinant FLNc d18-21 (#) are marked. For identification of FILIP a gel band at approx. 130 kDa was cut from each lane as indicated and analyzed by LC-MS. FILIP1 was unambigously identified in the pulldown with FLNc d18-21, but not FLNc d1-3 as illustrated by the respective LFQ-based intensity bar chart. Myh8, Myosin-8 **h.** Identification of endogenous FLNc in FILIP1 CT pull-down by LC-MS analysis. FLNc was identified with a sequence coverage of 78%. Identified peptides are shown in red.

Supplementary Figure 9

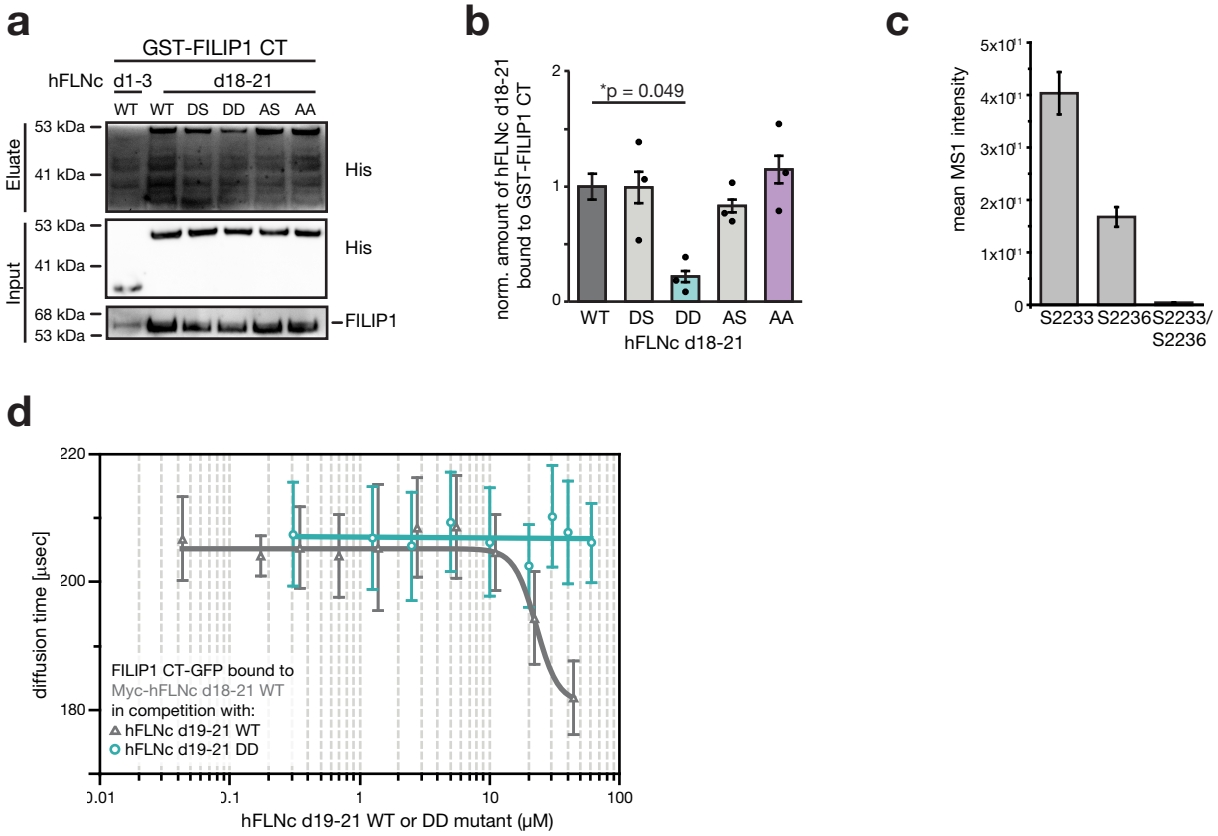

Supplementary Figure 9. Analysis of FILIP1 binding to human (h) FLNc in dependency of S2233/S2236 phosphorylation. **a.** Pull-down experiments using GST-FILIP1 CT as bait and His_6-tagged hFLNc d18-21 wild-type or S2233/S2236 phosphosite mutants as prey as indicated. Wild-type hFLNc d1-3 served as negative control. WT, wild-type; CT, carboxy-terminus; d, domain. **b.** Quantification of immunoblot data shown in (a). Calculated signal intensities were normalized to hFLNc d18-21. SEMs were calculated and a two-tailed student's t-test was performed (n = 3 independent experiments; *p ≤ 0.05). **c.** Mean MS intensities of phosphopeptides derived from recombinantly expressed hFLNc d18-21 in HEK293T cells. Peptides phosphorylated at S2233, S2236 or both 2233 and S2236 were summed and for each the mean MS1 intensity is shown (n=3 independent experiments, ± SEM). **d.** Fluorescence correlation spectroscopy analysis of co-expressed FILIP CT-GFP and Myc-hFLNc d18-21 in competition with recombinantly expressed hFLNc d19-21 WT (Kd = 22.85 + 2.86 µM) and hFLNc d19-21 DD mutant (Kd = n.a.), respectively. Data of 3 independent experiments are shown.

Supplementary Figure 10 area in boxes shown in Fig. 6f

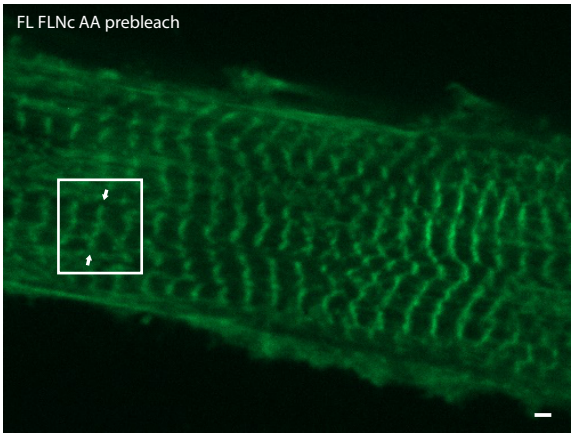

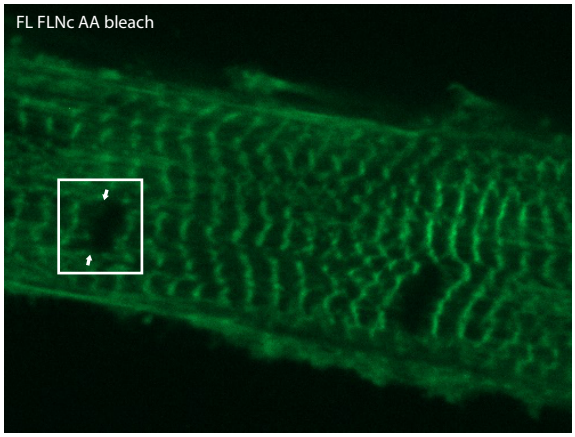

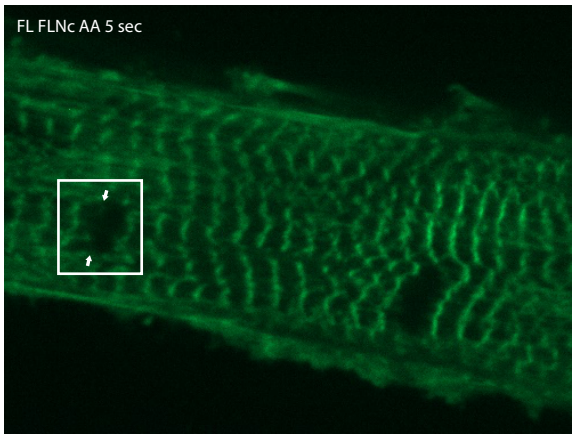

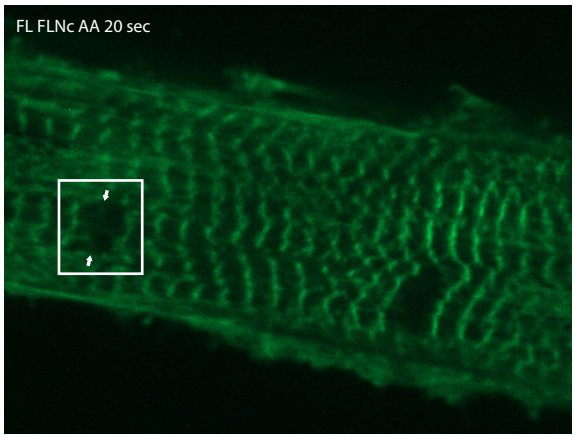

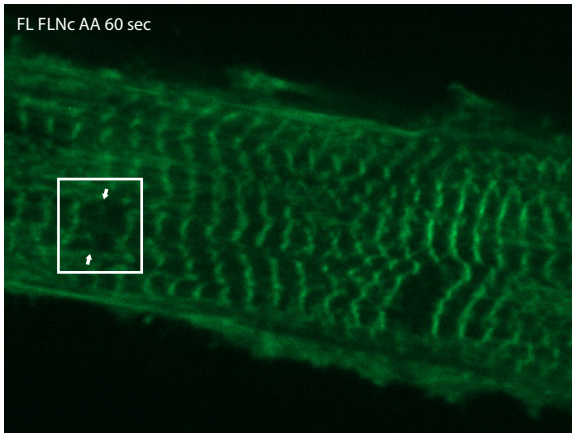

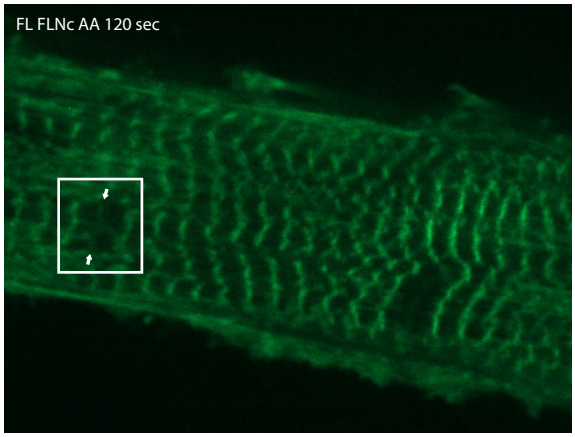

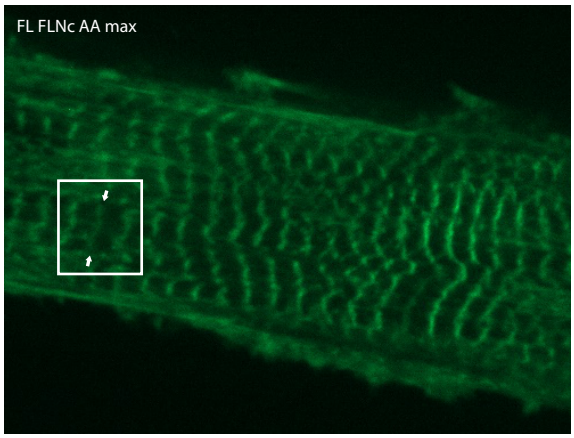

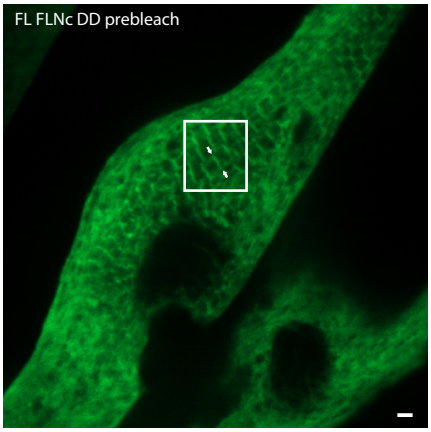
FL FLNc DD prebleach

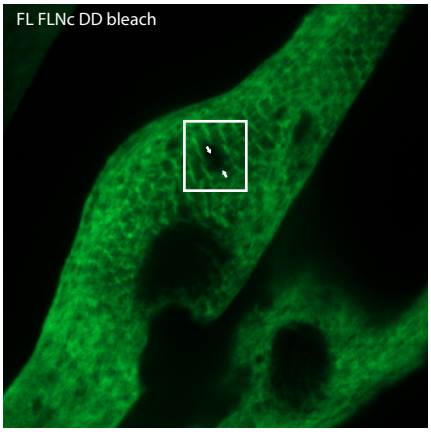
FL FLNc DD bleach

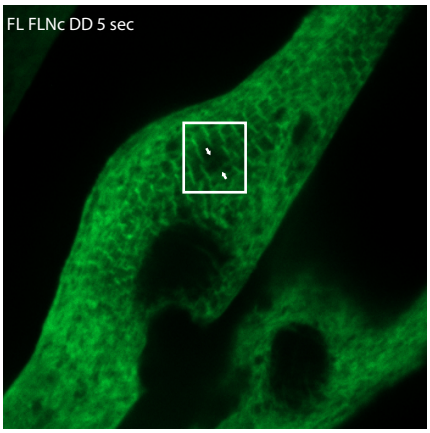
FL FLNc DD 5 sec

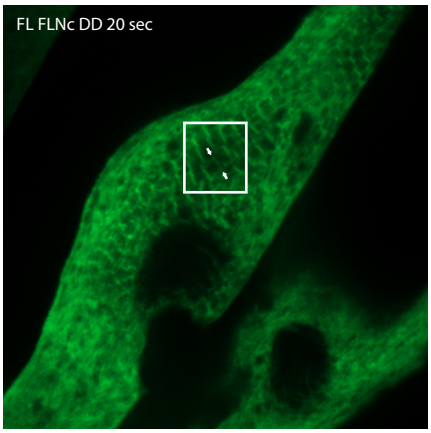
FL FLNc DD 20 sec

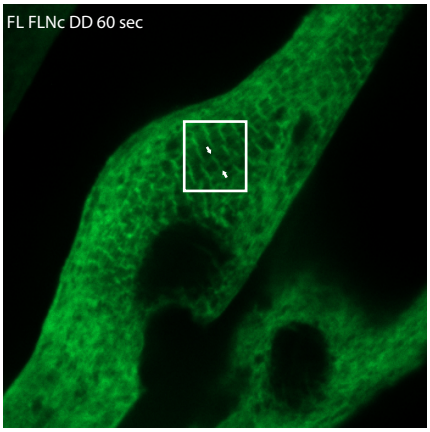
FL FLNc DD 60 sec

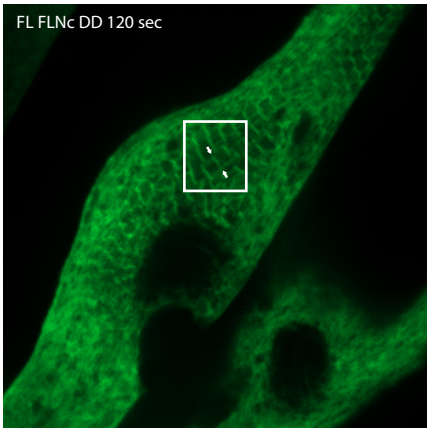
FL FLNc DD 120 sec

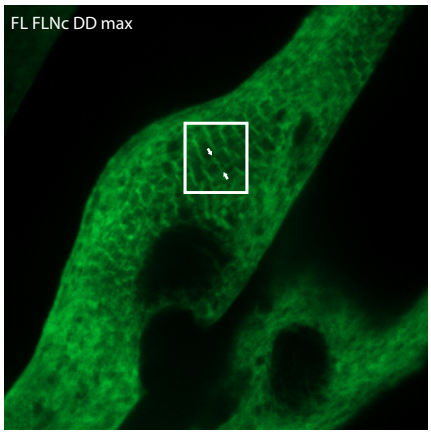
FL FLNc DD max

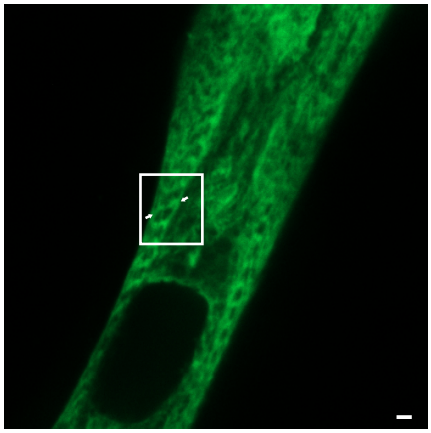

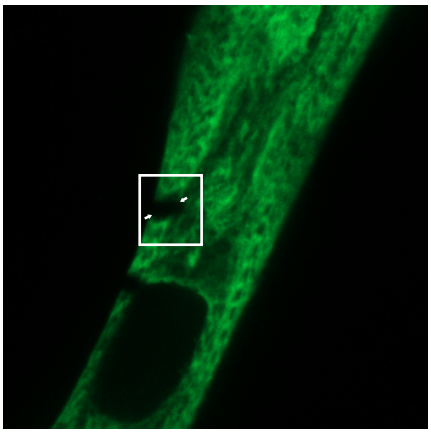

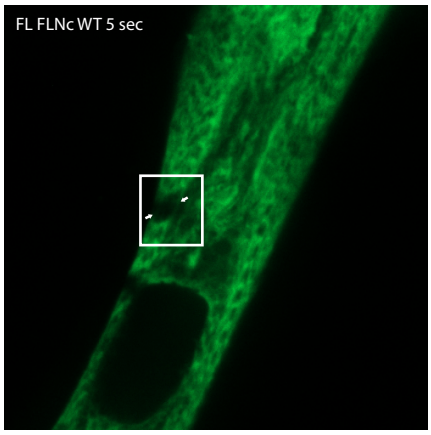

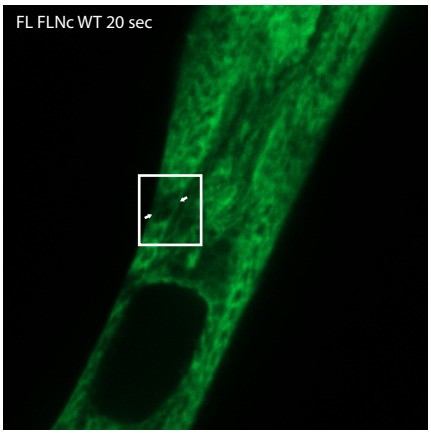

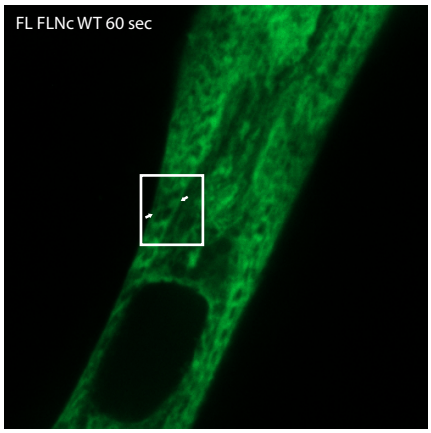

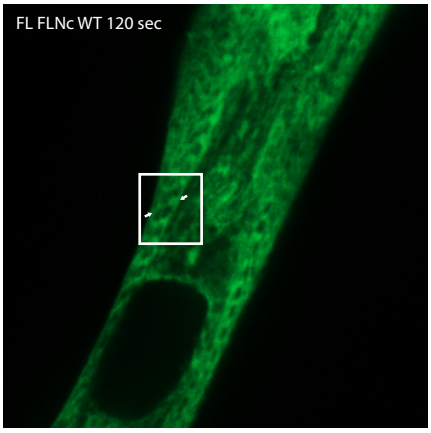

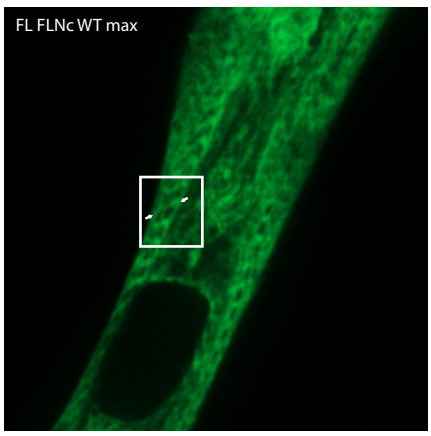

Supplementary Figure 10. Uncropped microscopic data from fluorescence recovery after photobleaching (FRAP) experiments, shown in Fig. 6f.

Supplementary Figure 11

shown in Fig. 7c

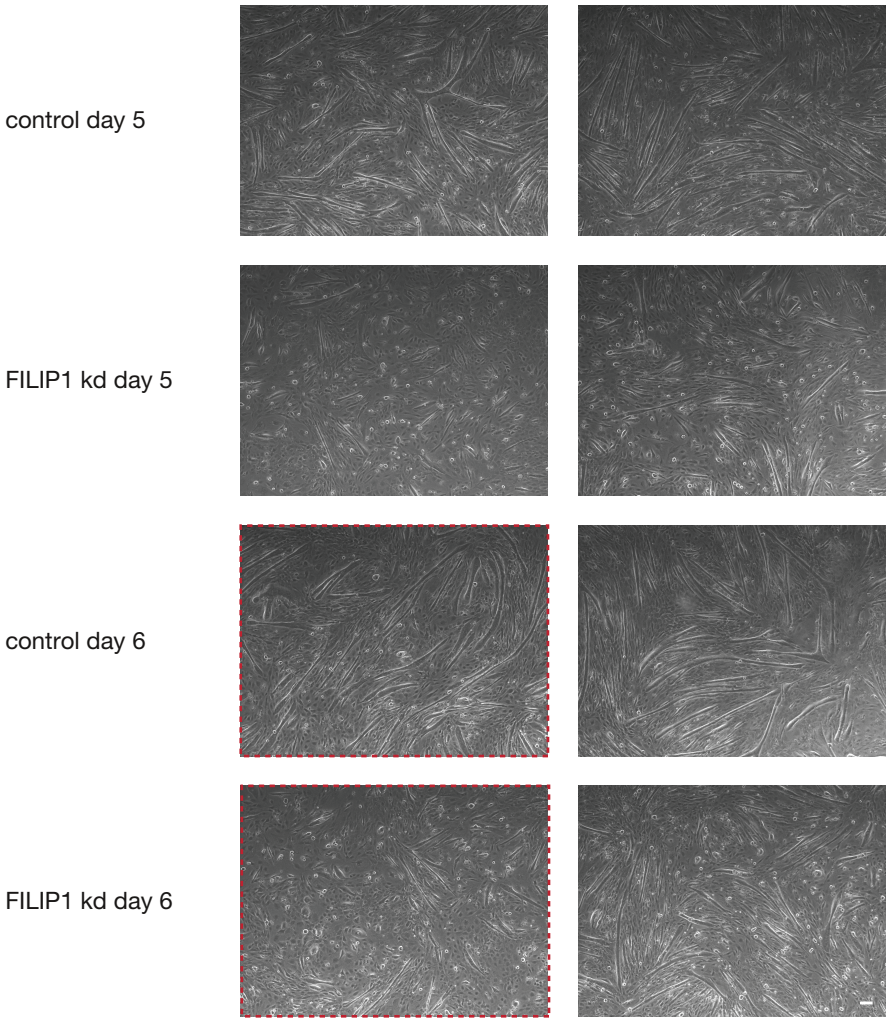

Supplementary Figure 11. Uncropped bright-field microscopy images from FILIP1 knockdown or control C2C12 cells, shown in Fig. 7c.

Supplementary Figure 12 area in boxes shown in Fig. 7d

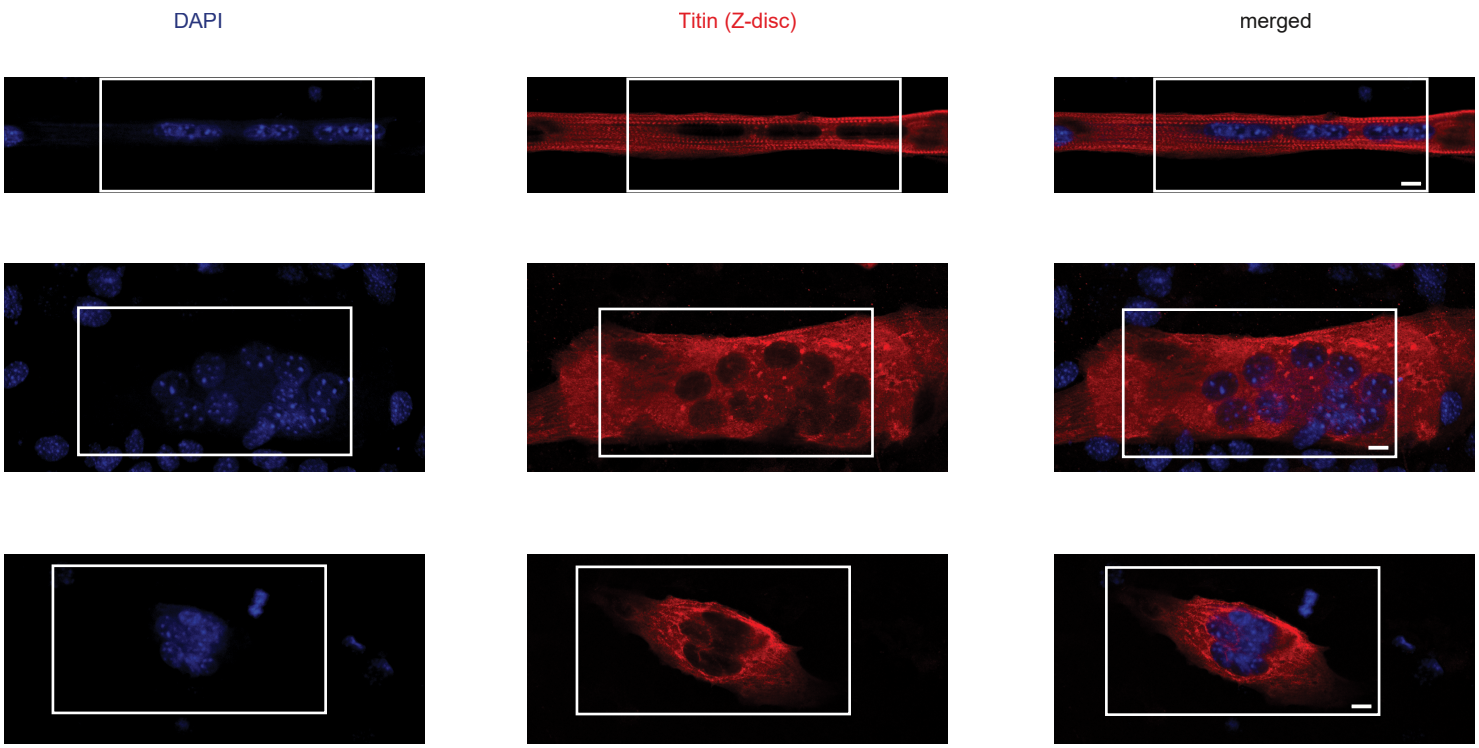

Supplementary Figure 12. Uncropped fluorescence microscopy images of FILIP1 knockdown or control C2C12 cells, shown in Fig. 7d.

Supplementary Figure 13

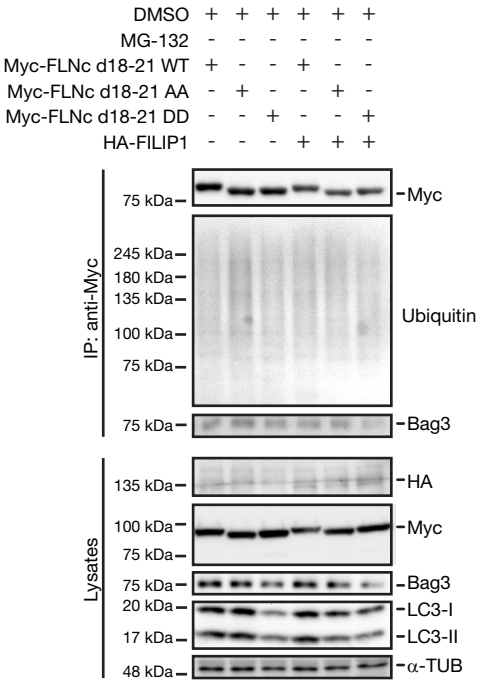

Supplementary Figure 13: Immunoblot analysis of control samples performed for experiment shown in Figure 7h. C2 cells were transfected with FLNc d18-21 WT or mutant forms in the presence or absence of HA-FILIP1. Cells were treated 6 h with DMSO before lysis and anti-Myc IP was performed. The first lane of the immunoblot corresponds to the last lane of the immunoblot shown in Figure 7h.